Performance of Integrated Ground-Air-Space FSO Links Over Various Turbulent Environments

Yalçın Ata and Mohamed-Slim Alouini, *Fellow, IEEE*

***Abstract*—We analyze the outage probability of integrated ground-air-space free-space optical (FSO) communication links for different atmospheric turbulence channel models. The performance of ground to high altitude platforms (HAPS), HAPS to geostationay Earth orbit (GEO) satellite, HAPS to HAPS and ground to GEO satellite is investigated for various link configurations (downlink, horizontal, and uplink) and parameters such as zenith angle, channel state, horizontal and vertical deviations, altitude, beam waist, receiver aperture diameter, wind speed, and visibility. The atmospheric attenuation (the effects of fog, cloud and volcanic activities), atmospheric turbulence, angle of arrival (AOA) fluctuations and pointing error are included in the considered model. Closed-form expressions for the probability density function (PDF) and cumulative distribution function (CDF) are obtained for Lognormal, Gamma and exponentiated Weibull distributed channel models. The benefit of using HAPS is shown by comparison of outage probabilities for direct ground to GEO satellite and HAPS assisted ground to GEO satellite links.**

***Index Terms*—Free-space optical communication, probability of outage, slant path and horizontal links, high altitude platforms, satellite communications.**

I. Introduction

AIR and space based applications are increasingly emerging in various areas and the demand for communication links of these applications having high data rates is rising. Since optical beam significantly suffers from atmospheric turbulence and environmental conditions, free-space optical (FSO) communication has found distance and weather limited usage in general. However, researchers are working for FSO based communication solutions to meet the need for high data rates. Besides some atmospheric turbulence mitigation techniques such as aperture averaging, adaptive optics (AO) correction and using multiple-input multiple-output (MIMO) systems; high altitude platforms (HAPS) relayed both hybrid radio frequency (RF)/FSO and only FSO links have become a prominent alternative in terms of increasing the performance of the wireless communication systems. In this frame, the concept of using HAPS to enhance the performance of terrestrial based and satellite wireless communication systems was discussed and system architectures for some applications were presented [1]. The advantegous the HAPS relayed satellite RF and FSO link was examined for the link budget and it was shown that the improvement in the performance can be up to 30 dB for HAPS relayed geostationary Earth orbit (GEO) satellite link [2]. Moreover, the cost effectivity of using HAPS instead of using many terrestrial base stations in terms of covering larger area was discussed [3]. A multi-hop HAPS assisted ground to ground network communication was analyzed and it was shown that the average bit-error-rate (BER), channel capacity and link availability of the communication system improve with the HAPS application and increased number of hops [4]. In [5], an unmanned aerial vehicle (UAV)-enabled mobile relaying for ground to ground communication was investigated and it was concluded that the larger link gains (or less path losses) are obtained for mobile UAV rather than static UAV. Link budget analysis of vertical backhaul and fronthaul for 5G+ application was performed in [6] depending on the different weather conditions. In addition to the significant influence of the some weather conditions, the key role of the divergence angle was shown with the multi Gb/s data rates with the reduced divergence angle. It was shown that the impact of atmospheric turbulence becomes negligible for downlink and uplink communication between GEO satellite and UAV at a certain altitude [7]. The effects of the angle of arrival (AOA) fluctuations and pointing error on the performance of the high altitude HAPS to HAPS link was studied in [8] and an adaptive beam control algorithm was proposed to define the optimum beam size and avoid the link loss. In [9], the performance analysis for ground to HAPS link including AOA fluctuations, pointing error and atmospheric turbulence channel with Lognormal and Gamma-Gamma distribution was studied. The misalignment errors in [9], which are assumed to be identical in both vertical and horizontal axes, are represented by Rayleigh distribution. A similar approach was used for a UAV-relayed FSO communication system in the Lognormal distributed turbulent channel in [10]. A compherensive survey was published to emphasize the opportunities, challenges, and unexplored potentials of the HAPS and their future deployments [11]. In [12], we analysed the performance of ground to HAPS downlink and uplink FSO communication systems in Gamma-Gamma distributed turbulent channel model and mitigation of the turbulence effect by applying adaptive optics correction. In this study, we make contribution by using different channel models (Lognormal, Gamma and exponentiated

Manuscript received 23 October 2022; accepted 27 October 2022. Date of publication 31 October 2022; date of current version 10 November 2022. *(Corresponding author: Yalçın Ata.)*

Yalçın Ata is with the Department of Electrical and Electronics Engineering, OSTIM Technical University, 06374 Ankara, Turkey (e-mail: ylcnata@gmail.com).

Mohamed-Slim Alouini is with the Computer, Electrical, and Mathematical Sciences and Engineering (CEMSE) Division, King Abdullah University of Science and Technology (KAUST), Thuwal, Makkah 23955-6900, Kingdom of Saudi Arabia (e-mail: slim.alouini@kaust.edu.sa).

Digital Object Identifier 10.1109/JPHOT.2022.3218512

Weibull) and extending the communication link from ground station (GS) to GEO satellite both directly and using HAPS relaying. We also did not include adaptive optics correction effect but accounted for aperture averaging in this study.

Regarding integrated ground-air-space network application, the error probability of a HAPS assisted relaying using hybrid RF/FSO communication system has been analyzed recently [13]. The better performance with the HAPS relaying ground to satellite link was obtained compared with the direct ground to satellite link. A novel hybrid RF/FSO satellite communication system was offered to improve the usability of FSO link and the importance of the zenith-angle dependency for system design was concluded [14].

All above mentioned studies show that the performance of the integrated ground to air or satellite FSO communication systems is degraded considerably with the weather conditions (especially foggy weather), atmopsheric turbulence, pointing error and AOA fluctuations due to the hovering aerial vehicle. However, HAPS assisted links improve the performance of communication systems up to certain level. It is obvious that more detailed analyzes are needed from different perspectives for accurate modeling and optimum deployment of different communication link configurations. Our motivation is to investigate the performance of slant path and horizontal links in both direct and HAPS assisted applications in various turbulence environments modeled by different channel distributions. There are several channel models which are used to characterize the turbulent channel statistics such as Lognormal, Gamma, Gamma-Gamma, exponentiated Weibull and K-distribution. Among these models, Lognormal and Gamma-Gamma channel models are widely adopted to model turbulent channels. In our previous study [12], we investigated the Gamma-Gamma distribution model for ground to HAPS communication link in different aspects. In this study, our motivation is to extend our previous study and reflect the behaviour of the ground to satellite communication links and relay applications in different turbulence channel models. Although the Lognormal channel model is partially effective in stronger turbulence with a sufficiently large receiver, it generally yields quite effective results for a point receiver operating in weak turbulence conditions [15], [16], [17]. Gamma distribution is presented to have highly effective approximation when the propagation is analyzed in terms of intensity and amplitude variations [18]. Exponentiated Weibull distribution, that is the generalized version of the Weibull distribution with a shape parameter, is shown to be yielding accurate results from weak-to-strong turbulence conditions with all aperture averaging variations [15]. However, it is obvious that each model has limitations under certain conditions and parameters. Due to these limitations, in direct and/or HAPS assisted ground-air-space applications, it becomes very important to reveal the performances of the above-mentioned models and validate their accuracy in the turbulent environment, and to compare the suitability and performance of these models to each other. For this purpose, we derived closed-form expressions for probability density function (PDF), cumulative distribution function (CDF) and probability of outage for FSO communication systems operating in Lognormal, Gamma and exponentiated Weibull distributed turbulent channels. Also, pointing error, AOA fluctuations and attenuations resulting from weather conditions, clouds and volcanic activities in troposphere and stratosphere regions are included in the considered model.Orientation deviations are modeled with Hoyt distribution assuming vertical and horizontal deviations can be asymmetric. The contribution of different parameters of turbulent environment, communication system and optical beam on the performance of FSO links is presented. The comparison of both direct and HAPS assisted ground to GEO satellite links is given. Also, the comparison of Lognormal, Gamma and exponentiated Weibull distribution under same conditions is presented.

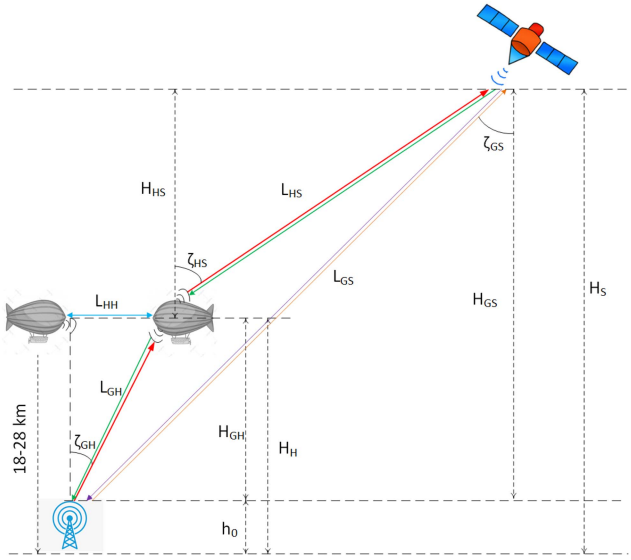

Fig. 1. System model.

From here on the paper is formed as follows. In Section II, the system model is given. Atmospheric attenuation is defined and channel model for Lognormal, Gamma and exponentiated Weibull distribution is given in Section III using turbulence parameters for various links. The effects of pointing error with Hoyt distribution and AOA fluctuations with Rayleigh model are also given in Section III. The outage performance analysis is performed in Section IV for all these channel models. Results are presented and discussed in Section V. Conclusion of our study is given in Section VII. Finally, the procedures used to obtain analytical expressions for channel models are offered in Appendix A, B, and C.

Table I lists the used symbols and their definitions.

II. System Model

The block diagram of the integrated ground-air-space communication systems is given in Fig. 1. All link configurations between ground to GEO satellite, HAPS to GEO satellite and ground to HAPS are assumed to be FSO based and, single transmitter and single receiver are used on both sides. The receiver is assumed to use aperture averaging [18]. The atmospheric turbulence is taken into account for three different models; Lognormal, Gamma and exponentiated Weibull distributed

TABLE I
LIST OF SYMBOLS

Symbol	Definition
ζ	Zenith angle
ζ_{GH}	Zenith angle for ground to HAPS link
ζ_{GS}	Zenith angle for ground to satellite link
ζ_{HS}	Zenith angle for HAPS to satellite link
η_s	Normalized beam waist with respect to σ_s
θ_d	Orientation deviation
θ_{FOV}	Field of view
Θ_0	Beam curvature parameter at the transmitter
Θ_1	Beam curvature parameter at the receiver
$\overline{\Theta}_1$	Complementary parameter
κ	Magnitude of the spatial frequency
λ	Wavelength
Λ_0	Fresnel ratio of Gaussian beam at transmitter
Λ_1	Fresnel ratio of Gaussian beam at receiver
ξ	Normalized distance parameter
σ_0	Variance of orientation deviation
σ_s	Displacement in polar s coordinates
σ_z	Displacement in polar z coordinates
σ^2_{lnX}	Large-scale log variance
σ^2_{lnY}	Small-scale log variance
Φ_n	Turbulence power spectrum
A	Nominal value of ground turbulence
σ	Attenuation coefficient
D_G	Receiver aperture diameter
F_0	Phase front radius of curvature
h	Channel state
h_0	Height of ground station
h_{af}	Angle of arrival
h_{al}	Attenuation loss
h_{at}	Atmospheric turbulence
h_{pl}	Pointing error
h_{th}	Threshold for channel state
H	Altitude
H_H	Altitude of HAPS
H_S	Altitude of satellite
H_{GH}	Height between ground station and HAPS
H_{GS}	Height between ground station and satellite
H_{HS}	Height between HAPS and satellite
k	Wavenumber
l	Height parameter
L	Link length
L_{GH}	Link length for ground to HAPS link
L_{GS}	Link length for ground to satellite link
L_{HH}	Link length for HAPS to HAPS link
L_{HS}	Link length for HAPS to satellite link
q	Visibility parameter
q_H	Ratio of vertical and horizontal deviations
r_a	Receiver aperture radius
V	Visibility
W_0	Gaussian beam radius
w	Wind speed
ω_b	Beam waist

TABLE II
EFFECT OF FOG CONDITIONS ON THE VISIBILITY AND ATTENUATION COEFFICIENT FOR $\lambda = 1550$ NM

Fog	$V(km)$	$\sigma(dB/km)$
thin	1.9	4.5859
light	0.77	16.6717
moderate	0.50	33.9618
thick	0.2	84.9046
dense	0.05	339.6183

channels. The performances of various slant path (downlink and uplink) links between GEO satellite and GS, HAPS to GEO satellite and GS to HAPS are investigated. Also, the performance of horizontal link between HAPS to HAPS is analyzed. Besides atmospheric turbulence, pointing error, AOA fluctuations, atmospheric attenuation, cloud attenuation and attenuation due to volcanic activities are included in the considered model. The comparison of direct GS to GEO satellite and HAPS assisted GS to GEO satellite links is presented to see the benefit of using HAPS. The details of the channel model are given below.

III. CHANNEL MODELS

A. Atmospheric Attenuation

The contribution of absorption and scattering to the optical beam attenuation in the atmosphere can be expressed by Beer-Lambert law as

$$h_{al} = \exp(-\sigma L), \tag{1}$$

where σ is the attenuation coefficient and L is the link length. The attenuation coefficient σ in (1) is obtained as follows depending on the visibility [19]

$$\sigma = \frac{3.912}{V}\left(\lambda/550\right)^{-q}, \tag{2}$$

where V is the visibility (in Km), λ is the wavelength (in nm), and the parameter q is expressed using the Kim model as

$$q = \begin{cases} 1.6, & V > 50\,\text{Km} \\ 1.3, & 6\,\text{Km} < V < 50\,\text{Km} \\ 0.16V + 0.34, & 1\,\text{Km} < V < 6\,\text{Km} \\ V - 0.5, & 0.5\,\text{Km} < V < 1\,\text{Km} \\ 0, & V < 0.5\,\text{Km} \end{cases}. \tag{3}$$

The visibility and attenuation coefficient of various fog conditions for $\lambda = 1550$ nm is given in Table II [20].Clouds also cause attenuation in atmosphere. The attenuation due to the clouds is modeled by using liquid water concentration (LWC) and cloud number concentration (CNC) and, the visibility is obtained by [21]

$$V = \frac{1.002}{(LWC \times CNC)^{0.6473}}. \tag{4}$$

The visibility and attenuation for various cloud types are given in Table III [20].

Another attenuation factor affecting the optical beam propagation is the stratospheric attenuation that is mainly caused by

TABLE III
THE VISIBILITY AND ATTENUATION COEFFICIENT IN DIFFERENT CLOUD TYPES FOR $\lambda = 1550$ NM

Cloud	CNC	LWC	V	σ
thin cirrus	0.5	3.31×10^{-4}	290.6970	0.0006
cirrus	0.025	0.06	64.6600	0.0026
altostrastus	400	0.41	0.0369	4.6019
stratocumulus	250	0.15	0.0959	1.7707
nimbostratus	200	0.65	0.0429	3.9583
cumulus	250	1.00	0.0280	6.0646
stratus	250	0.29	0.0626	2.7126

[a] $CNC(cm^{-3})$, $LWC(g/m^{-3})$, $V(km)$, $\sigma(\times 10^5 dB/km)$.

TABLE IV
THE ATTENUATION FOR DIFFERENT VOLCANIC ACTIVITIES

Stratospheric Model	Attenuation (km^{-1})
Extreme volcanic activiy	4×10^{-3}
High volcanic activiy	1×10^{-3}
Moderate volcanic activiy	1×10^{-4}

volcanic activities. The attenuation for various volcanic activiy types is given in Table IV [22].

B. Atmospheric Turbulence for Different Paths

1) Rytov Variance: The profile of structure parameter for refractive index fluctuation is expressed as ([18], p. 481)

$$C_n^2(l) = 0.00594\left(\frac{w}{27}\right)^2 (10^{-5}l)^{10}\exp\left(-\frac{l}{1000}\right) + 2.7\times 10^{-16}\exp\left(-\frac{l}{1500}\right) + A\exp\left(-\frac{l}{1000}\right), \tag{5}$$

in Hufnagel-Valley (HV) model, where l is the parameter of height, w denotes the root mean square (rms) of the wind speed in m/s, A is the turbulence structure constant at the ground level ($C_n^2(0)$) in $m^{-2/3}$ varying with the wind speed in the HV5/7 model. Then, the power spectrum of the turbulence based on the Kolmogorov theory becomes

$$\Phi_n(\kappa, l) = 0.033 C_n^2(l)\kappa^{-11/3}, \tag{6}$$

where κ is the spatial wave number. Being valid for weak, moderate and strong turbulence conditions; the scintillation index is [18] (p. 420)

$$\sigma_I^2 = \exp\left[\sigma_{lnX}^2(D_G) + \sigma_{lnY}^2(D_G)\right] - 1, \tag{7}$$

where D_G is the receiver aperture diameter, σ_{lnX}^2 and σ_{lnY}^2 are the large- and small-scale log variances respectively and they are defined as

$$\sigma_{lnX}^2 = 0.49\left(\frac{\Omega_G - \Lambda_1}{\Omega_G + \Lambda_1}\right)^2 \sigma_{Bi}^2 / \left[1 + 0.56(1+\Theta_1)\sigma_{Bi}^{12/5} + \frac{0.4(2-\overline{\Theta}_1)(\sigma_{Bi}/\sigma_{Ri})^{12/7}}{(\Omega_G + \Lambda_1)\left(1/3 - 0.5\overline{\Theta}_1 + 0.2\overline{\Theta}_1^2\right)^{6/7}}.\right]^{7/6}, \tag{8}$$

$$\sigma_{lnY}^2 = \frac{0.51\sigma_{Bi}^2\left(1 + 0.69\sigma_{Bi}^{12/5}\right)^{-5/6}}{1 + \left[1.20(\sigma_{Ri}/\sigma_{Bi})^{12/5} + 0.83\sigma_{Ri}^{12/5}\right]/(\Omega_G + \Lambda_1)}, \tag{9}$$

where index i is $i \in d, u, h$ depending on the downlink, uplink and horizontal link communication, $\Omega_G = 2\,L/(kW_G^2)$ is the non-dimensional Fresnel parameter, W_G is the radius of Gaussian lens and $W_G^2 = D_G^2/8$, $\Lambda_0 = 2\,L/(kW_0^2)$, W_0 is the beam radius, $\Lambda_1 = \Lambda_0/(\Lambda_0^2 + \Theta_0^2)$ is the Fresnel ratio of Gaussian beam at receiver, F_0 is the phase front radius of curvature, $\Theta_0 = 1 - L/F_0$ and $\Theta_1 = \Theta_0/(\Lambda_0^2 + \Theta_0^2)$ are the beam curvature parameters at the transmitter and transmitter, $\overline{\Theta}_1 = 1 - \Theta_1$ is the complementary parameter. In (8) and (9), σ_{Bi}^2 and σ_{Ri}^2 are the Rytov variances for Gaussian beam and plane wave.

a) Slant Path Links: The Rytov variance of Gaussian beam propagating in slant path link is [18]

$$\sigma_B^2 = 8\pi^2 k^2 sec(\zeta)\int_{h_0}^{H}\int_0^{\infty}\kappa\Phi_n(l,\kappa)\exp\left(-\Lambda_1 L\kappa^2\xi^2/k\right) \times \mathrm{Re}\left\{1 - \exp\left[i\frac{\kappa^2 L}{k}\xi\left(1 - \overline{\Theta}_1\xi\right)\right]\right\} d\kappa\, dl, \tag{10}$$

where $k = 2\pi/\lambda$ is the wavenumber, ζ is the zenith angle, ξ is the normalized distance parameter, h_0 is the height of the ground station, H is the altitude of air or space platform, and Re denotes the real part. The normalized distance parameter of the downlink is $\xi = \frac{(l-h_0)}{(H-h_0)}$. Using (10), the Rytov variances for a Gaussian beam and plane wave in downlink are obtained as [18],

$$\sigma_{Bd}^2 = 8.70k^{7/6}(H-h_0)^{5/6}sec^{11/6}(\zeta)\mathrm{Re}\left(\int_{h_0}^{H} C_n^2(l) \times \left\{\left[\Lambda\xi^2 + i\xi\left(1 - \overline{\Theta}\xi\right)\right]^{5/6} - \Lambda^{5/6}\xi^{5/3}\right\} dl\right), \tag{11}$$

$$\sigma_{Rd}^2 = 2.25k^{7/6}sec^{11/6}(\zeta)\int_{h_0}^{H} C_n^2(l)\,(l-h_0)^{5/6}\,dl. \tag{12}$$

In uplink case, $\xi = 1 - \frac{(l-h_0)}{(H-h_0)}$. Then, the Rytov variance for uplink is [18]

$$\sigma_{Bu}^2 = 8.70k^{7/6}(H-h_0)^{5/6}sec^{11/6}(\zeta)\mathrm{Re}\left(\int_{h_0}^{H} C_n^2(l) \times \left\{\left[\Lambda\xi^2 + i\xi\left(1 - \overline{\Theta}\xi\right)\right]^{5/6} - \Lambda^{5/6}\xi^{5/3}\right\} dl\right). \tag{13}$$

On setting $\Theta_1 = 1$ and $\Lambda_1 = 0$ in (13), the Rytov variance of plane wave for uplink can be obtained as

$$\sigma_{Ru}^2 = 2.25k^{7/6}sec^{11/6}(\zeta)\int_{h_0}^{H} C_n^2(l)\,(H-l)^{5/6}\,dl. \tag{14}$$

b) Horizontal Path Link: The Rytov variance of a Gaussian beam for horizontal link is [18]

$$\sigma_{Bh}^2 = 8\pi^2 k^2 L \int_0^1 d\xi \int_0^\infty \kappa \Phi_n(l,\kappa) \exp\left(-\Lambda_1 L \kappa^2 \xi^2/k\right) \times \mathrm{Re}\left\{1 - \exp\left[i\frac{\kappa^2 L}{k}\xi\left(1-\overline{\Theta}_1\xi\right)\right]\right\} d\kappa\, dl. \quad (15)$$

Since the height is constant for horizontal FSO link, the refractive index structure parameter $C_n^2(l)$ given in (5) will also keep its constant value for fixed l over link length. Then, the Rytov variance of propagating Gaussian beam can be obtained by using (13) as

$$\sigma_{Bh}^2 = 4.75 C_n^2(l) k^{\frac{7}{6}} L^{\frac{11}{6}} \left\{0.40\left[\left(1+2\Theta_1\right)^2 + 4\Lambda_1^2\right]^{\frac{5}{12}} \times \cos\left[\frac{5}{6}\tan^{-1}\left(\frac{1+2\Theta_1}{2\Lambda_1}\right)\right] - \frac{11}{16}\Lambda_1^{5/6}\right\}. \quad (16)$$

And, the Rytov variance of plane wave for horizontal link will be $\sigma_{Rh}^2 = 1.23 C_n^2(l) k^{7/6} L^{11/6}$.

2) Different Turbulence Channel Models: Here, the different types of channel models are given to characterize the atmospheric turbulence-induced fluctuations.

a) Lognormal Distributed Channel Model: The PDF of the Lognormal channel model is expressed by [18]

$$f_{h_{at}}(h_{at}) = \frac{1}{h_{at}\sqrt{2\pi\sigma_l^2}} \exp\left\{-\frac{\left[ln(h_{at}) + 0.5\sigma_l^2\right]^2}{2\sigma_l^2}\right\}, \quad (17)$$

where $h_{at} > 0$ is the channel state for atmospheric turbulence and $\sigma_l^2 = ln(\sigma_I^2 + 1)$ is the log-irradiance variance.

b) Gamma Distributed Channel Model: The PDF of the Gamma distributed channel model is [23]

$$f_{h_{at}}(h_{at}) = \frac{1}{\Gamma(k)\theta^k} h_{at}^{k-1} \exp(-h_{at}/\theta), h_{at} > 0, \quad (18)$$

where $\theta = \sigma_I^2$ and $k = 1/\sigma_I^2$. If $k = 1$, then the Gamma distribution becomes negative exponential distribution.

c) Exponentiated Weibull Distributed Channel Model: The PDF of the exponentiated Weibull distributed channel model is [15]

$$f_{h_{at}}(h_{at}) = \frac{\alpha\beta}{\eta}\left(\frac{h_{at}}{\eta}\right)^{\beta-1} \exp\left[-\left(\frac{h_{at}}{\eta}\right)^{\beta}\right] \times \left\{1 - \exp\left[-\left(\frac{h_{at}}{\eta}\right)^{\beta}\right]\right\}^{\alpha-1}, h_{at} > 0, \quad (19)$$

and $\beta \approx 1.012(\alpha\sigma_I^2)^{-13/25} + 0.142, \alpha > 0$ is the shape parameter and is given by $\alpha \cong 7.22\sigma_I^{2/3}/\Gamma(2.487\sigma_I^{2/6} - 0.104)$ and $\eta = 1/[\alpha\Gamma(1+1/\beta)g_1(\alpha,\beta)]$ and $g_n(\alpha,\beta)$ is given by

$$g_n(\alpha,\beta) = \sum_{i=0}^{\infty} \frac{(-1)^i \Gamma(\alpha)}{i!(i+1)^{1+n/\beta}\Gamma(\alpha-i)}, \quad (20)$$

where 10 or less terms are sufficient for series to be converged. We note that when $\alpha = 1$, exponentiated Weibull distribution becomes Weibull distribution.

C. Pointing Error

Assuming that the jitter variances over the two dimensions are not identical, the PDF of the misalignment by Hoyt distribution for the orthogonal directions s and z is [24]

$$f_{s,z}(s,z) = \frac{1}{2\pi q_H \sigma_s^2} \exp\left(-\frac{q_H^2 s^2 + z^2}{2q_H^2\sigma_s^2}\right), \quad (21)$$

where $q_H = \sigma_z/\sigma_s$ varying in interval (0,1], σ_s and σ_z are the jitter variances in both directions. Using the relationships $s = r\cos(\varphi)$ and $z = r\sin(\varphi)$ for polar coordinates, PDF takes the form [24]

$$f_{r,\varphi}(r,\varphi) = \frac{r}{2\pi q_H \sigma_s^2} \exp\left(-\frac{r^2\xi(\varphi)}{2q_H^2\sigma_s^2}\right), \quad (22)$$

where

$$\xi(\varphi) = \frac{1 - (1-q_H^2)\cos^2\varphi}{q_H^2}. \quad (23)$$

Then the PDF of the pointing error given in (21) is found to be [24]

$$f_{pl}(h_{pl}) = \frac{\eta_s^2}{2\pi q_H} \int_{-\pi}^{\pi} \frac{h_{pl}^{\eta_s^2\xi(\varphi)-1}}{A_0^{\eta_s^2\xi(\varphi)}} d\varphi, \quad (24)$$

where $\eta_s = \omega_e/(2\sigma_s)$, $\omega_e = \omega_b\sqrt{\sqrt{\pi}\mathrm{erf}(\upsilon)/(2\upsilon e^{-\upsilon^2})}$, ω_b is the beamwaist, erf(.) is error function, $\upsilon = \sqrt{\pi/2}r_a/\omega_b$, $r_a = D_G/2$ is the receiver aperture radius, and $A_0 = \mathrm{erf}^2(\upsilon)$. Including the deviation angle θ_d then, the conditional probability for the PDF of pointing error h_{pl} can be found

$$f_{pl|\theta_d}(h_{pl}) = \frac{\eta_s^2}{2\pi q_H} \int_{-\pi}^{\pi} \frac{h_{pl}^{\eta_s^2\xi(\varphi)-1}}{A_0^{\eta_s^2\xi(\varphi)}} \cos(\theta_d) d\varphi. \quad (25)$$

We note that (25) becomes $f_{pl|\theta_d}(h_{pl}) = \eta_s^2 \frac{h_{pl}^{\eta_s^2-1}}{A_0^{\eta_s^2}} \cos(\theta_d)$ for $q_H = 1$.

D. AOA Fluctuations

For small deviation angle in comparison to the field of view (FOV) ($\theta_d \le \theta_{FOV}$), the fading due to AOA fluctuations is expressed by [9]

$$h_{af} = 1 - \left[J_0\left(\frac{\pi r_a}{\lambda}\right)\right]^2 - \left[J_1\left(\frac{\pi r_a}{\lambda}\right)\right]^2, \quad (26)$$

where $J_n(.)$ is the n^{th} order Bessel function of the first kind. The PDF of random variable θ_d modeled by Rayleigh distribution is [9]

$$f_{\theta_d}(\theta_d) = \frac{\theta_d}{\sigma_0^2} \exp\left(-\frac{\theta_d^2}{2\sigma_0^2}\right), \theta_d \ge 0, \quad (27)$$

where σ_0^2 is the variance of random variable θ_d.

IV. Outage Probability Analysis

The outage probability of slant path (ground to HAPS, ground to GEO satellite, HAPS to GEO satellite) and horizontal (HAPS to HAPS) links is analyzed in this section. Taking into account all the effects mentioned above, the channel state for downlink, uplink and horizontal link can be written as

$$h = h_{al} h_{at} h_{pl} h_{af}, \tag{28}$$

where h_{al}, h_{at}, h_{pl}, and h_{af} represent the effects of the attenuation loss, atmospheric turbulence, pointing error, and AOA fluctuations, respectively. The conditional channel state on θ_d can be represented as

$$\begin{aligned} f_{h_{ag}|\theta_d}(h_{ag}) &= \int_{\frac{h_{ag}}{A_0 h_{al}}}^{\infty} f_{h_{ag}|\theta_d,h_{at}}(h_{at}) f_{h_{at}}(h_{at}) dh_{at} \\ &= \int_{\frac{h_{ag}}{A_0 h_{al}}}^{\infty} \frac{1}{h_{al} h_{at}} f_{h_{pl}|\theta_d}\left(\frac{h_{ag}}{h_{al} h_{at}}\right) f_{h_{at}}(h_{at}) dh_{at}, \end{aligned} \tag{29}$$

using the relationship as $h_{ag} = h_{al} h_{at} h_{pl}$.

A. Lognormal Distributed Channel Model

Inserting the PDF of the Lognormal channel model and the conditional probability of PDF of the pointing error given in (17) and (25) into (29); the PDF of h_{ag} conditioned on the deviation angle θ_d is found by

$$\begin{aligned} f_{h_{ag}|\theta_d}(h_{ag}) = \frac{\eta_s^2 \cos(\theta_d)}{2\pi q_H \sqrt{2\pi\sigma_l^2}} \int_{-\pi}^{\pi} \frac{h_{ag}^{\eta_s^2\xi(\varphi)-1}}{A_0^{\eta_s^2\xi(\varphi)} h_{al}^{\eta_s^2\xi(\varphi)}} d\varphi \\ \times \int_{\frac{h_{ag}}{A_0 h_{al}}}^{\infty} \frac{\exp\left\{-\frac{\left[ln(h_{at})+0.5\sigma_l^2\right]^2}{2\sigma_l^2}\right\}}{h_{at}^{\eta_s^2\xi(\varphi)+1}} dh_{at}. \end{aligned} \tag{30}$$

After derivations given in Appendix-A (A.1)–(A.8), the PDF of the channel state for Lognormal distribution will be obtained as

$$\begin{aligned} f_h(h) = \frac{\eta_s^2 \exp(-\sigma_l^2/8) \exp(-\sigma_0^2/2) h_{af1} F_1\left(-\frac{1}{2}, \frac{1}{2}; \frac{\sigma_0^2}{2}\right)}{4\pi q_H} \\ \times \int_{-\pi}^{\pi} \frac{h^{\eta_s^2\xi(\varphi)-1} \exp\left[\sigma_l^2 \left(\eta_s^2\xi(\varphi)+1/2\right)^2/2\right]}{A_0^{\eta_s^2\xi(\varphi)} h_{al}^{\eta_s^2\xi(\varphi)}} d\varphi \\ \times \left[1 - \text{erf}\left(\frac{ln(\frac{h}{A_0 h_{al}})}{\sqrt{2\sigma_l^2}} + \frac{\sqrt{2\sigma_l^2}\left(\eta_s^2\xi(\varphi)+1/2\right)}{2}\right)\right]. \end{aligned} \tag{31}$$

The CDF of the channel state h is expressed as follows depending on the PDF of the Lognormal distributed channel model

$$F_h(h) = \int_0^h f_h(x) dx. \tag{32}$$

Substituting (31) into (32), one can find the CDF of the Lognormal distributed channel as

$$\begin{aligned} F_h(h) = \frac{\eta_s^2 \exp(-\sigma_l^2/8) \exp(-\sigma_0^2/2) h_{af1} F_1\left(-\frac{1}{2}, \frac{1}{2}; \frac{\sigma_0^2}{2}\right)}{4\pi q_H} \\ \times \int_{-\pi}^{\pi} \frac{\exp\left[\sigma_l^2 \left(\eta_s^2\xi(\varphi)+1/2\right)^2/2\right]}{A_0^{\eta_s^2\xi(\varphi)} h_{al}^{\eta_s^2\xi(\varphi)}} d\varphi \int_0^h x^{\eta_s^2\xi(\varphi)-1} \\ \left[1 - \text{erf}\left(\frac{ln(\frac{x}{A_0 h_{al}})}{\sqrt{2\sigma_l^2}} + \frac{\sqrt{2\sigma_l^2}\left(\eta_s^2\xi(\varphi)+1/2\right)}{2}\right)\right] dx. \end{aligned} \tag{33}$$

Following the derivations given in Appendix-A (A.9)–(A.14), the CDF of the channel state h will be obtained as

$$\begin{aligned} F_h(h) = \frac{\exp(-\sigma_l^2/8) \exp(-\sigma_0^2/2) h_{af1} F_1\left(-\frac{1}{2}, \frac{1}{2}; \frac{\sigma_0^2}{2}\right)}{4\pi q_H} \\ \times \int_{-\pi}^{\pi} \exp\left[\frac{\sigma_l^2 \left(\eta_s^2\xi(\varphi)+1/2\right)^2}{2}\right] \frac{1}{\xi(\varphi)} \\ \times \exp\left[-\sigma_l^2 \eta_s^2 \xi(\varphi)\left(\eta_s^2\xi(\varphi)+1/2\right)\right] \left\{\exp\left[\eta_s^2\xi(\varphi)\right.\right. \\ \times \ln\left(\frac{h}{A_0 h_{al}}\right) + \sigma_l^2 \eta_s^2 \xi(\varphi)\left(\eta_s^2\xi(\varphi)+\frac{1}{2}\right)\left.\right] \\ + \exp\left(\sigma_l^2 \eta_s^4 \xi^2(\varphi)/2\right) \text{erfc}\left(\sqrt{2\sigma_l^2}\eta_s^2\xi(\varphi)/2\right) \\ - \exp\left(\sigma_l^2 \eta_s^4 \xi^2(\varphi)/2\right) \text{erf}\left(-\frac{ln(\frac{h}{A_0 h_{al}})}{\sqrt{2\sigma_l^2}} - \frac{\sqrt{2\sigma_l^2}}{4}\right) \\ + \exp\left(\sigma_l^2 \eta_s^4 \xi^2(\varphi)/2\right) \text{erf}\left(\sqrt{2\sigma_l^2}\eta_s^2\xi(\varphi)/2\right) \\ - \exp\left[\eta_s^2\xi(\varphi)\ln(\frac{h}{A_0 h_{al}}) + \sigma_l^2\eta_s^2\xi(\varphi)(\eta_s^2\xi(\varphi)+\frac{1}{2})\right] \\ \times \text{erf}\left(\frac{ln(\frac{h}{A_0 h_{al}})}{\sqrt{2\sigma_l^2}} + \frac{\sqrt{2\sigma_l^2}\left(\eta_s^2\xi(\varphi)+1/2\right)}{2}\right)\Bigg\} d\varphi. \end{aligned} \tag{34}$$

The probability of outage can be found by using the CDF as

$$P_{out} = P_r(h \le h_{th}) = F_h(h_{th}). \tag{35}$$

Substituting (34) in (35), the probability of outage will be

$$\begin{aligned} P_{out} = \frac{\exp(-\sigma_l^2/8) \exp(-\sigma_0^2/2) h_{af1} F_1\left(-\frac{1}{2}, \frac{1}{2}; \frac{\sigma_0^2}{2}\right)}{4\pi q_H} \\ \times \int_{-\pi}^{\pi} \exp\left[\frac{\sigma_l^2 \left(\eta_s^2\xi(\varphi)+1/2\right)^2}{2}\right] \frac{1}{\xi(\varphi)} \\ \times \exp\left[-\sigma_l^2 \eta_s^2 \xi(\varphi)\left(\eta_s^2\xi(\varphi)+1/2\right)\right] \\ \times \left\{\exp\left[\eta_s^2\xi(\varphi)\ln(\frac{h_{th}}{A_0 h_{al}}) + \sigma_l^2\eta_s^2\xi(\varphi)(\eta_s^2\xi(\varphi)+\frac{1}{2})\right]\right. \\ + \exp\left(\sigma_l^2 \eta_s^4 \xi^2(\varphi)/2\right) \text{erfc}\left(\sqrt{2\sigma_l^2}\eta_s^2\xi(\varphi)/2\right) \\ \left. - \exp\left(\sigma_l^2 \eta_s^4 \xi^2(\varphi)/2\right) \text{erf}\left(-\frac{ln(\frac{h_{th}}{A_0 h_{al}})}{\sqrt{2\sigma_l^2}} - \frac{\sqrt{2\sigma_l^2}}{4}\right)\right. \end{aligned}$$

$$+\exp\left(\sigma_l^2\eta_s^4\xi^2(\varphi)/2\right)\operatorname{erf}\left(\sqrt{2\sigma_l^2}\eta_s^2\xi(\varphi)/2\right)$$
$$-\exp\left[\eta_s^2\xi(\varphi)\ln(\frac{h_{th}}{A_0h_{al}})+\sigma_l^2\eta_s^2\xi(\varphi)(\eta_s^2\xi(\varphi)+\frac{1}{2})\right]$$
$$\times\operatorname{erf}\left(\frac{ln(\frac{h_{th}}{A_0h_{al}})}{\sqrt{2\sigma_l^2}}+\frac{\sqrt{2\sigma_l^2}\left(\eta_s^2\xi(\varphi)+1/2\right)}{2}\right)\Bigg\}d\varphi. \quad (36)$$

For the special case $q_H=1$, the closed-form expression of outage probability in (36) takes the form of

$$P_{out}=\frac{\exp(-\sigma_l^2/8)\exp(-\sigma_0^2/2)h_{af1}F_1\left(-\frac{1}{2},\frac{1}{2};\frac{\sigma_0^2}{2}\right)}{2}$$
$$\times\exp\left[\frac{\sigma_l^2\left(\eta_s^2+1/2\right)^2}{2}\right]\exp\left[-\sigma_l^2\eta_s^2\left(\eta_s^2+1/2\right)\right]$$
$$\times\Bigg\{\exp\left[\eta_s^2\ln\left(\frac{h_{th}}{A_0h_{al}}\right)+\sigma_l^2\eta_s^2\left(\eta_s^2+1/2\right)\right]$$
$$+\exp\left(\sigma_l^2\eta_s^4/2\right)\operatorname{erfc}\left(\sqrt{2\sigma_l^2}\eta_s^2/2\right)$$
$$-\exp\left(\sigma_l^2\eta_s^4/2\right)\operatorname{erf}\left(-\frac{ln(\frac{h_{th}}{A_0h_{al}})}{\sqrt{2\sigma_l^2}}-\frac{\sqrt{2\sigma_l^2}}{4}\right)$$
$$+\exp\left(\sigma_l^2\eta_s^4/2\right)\operatorname{erf}\left(\sqrt{2\sigma_l^2}\eta_s^2/2\right)$$
$$-\exp\left[\eta_s^2\ln\left(\frac{h_{th}}{A_0h_{al}}\right)+\sigma_l^2\eta_s^2\left(\eta_s^2+1/2\right)\right]$$
$$\times\operatorname{erf}\left(\frac{ln(\frac{h_{th}}{A_0h_{al}})}{\sqrt{2\sigma_l^2}}+\frac{\sqrt{2\sigma_l^2}\left(\eta_s^2+1/2\right)}{2}\right)\Bigg\}. \quad (37)$$

B. Gamma Distributed Channel Model

Inserting (18) and (25) into (29), we find the conditioned PDF of h_{ag} as

$$f_{h_{ag}|\theta_d}(h_{ag})=\frac{\eta_s^2\cos(\theta_d)}{2\pi q_H\Gamma(k)\theta^k}\int_{-\pi}^{\pi}\frac{h_{ag}^{\eta_s^2\xi(\varphi)-1}}{A_0^{\eta_s^2\xi(\varphi)}h_{al}^{\eta_s^2\xi(\varphi)}}d\varphi$$
$$\times\int_{\frac{h_{ag}}{A_0h_{al}}}^{\infty}h_{at}^{k-\eta_s^2\xi(\varphi)-1}\exp\left(-h_{at}/\theta\right)dh_{at}. \quad (38)$$

Then, following the procedures given in Appendix-B (B.1),(B.2), the PDF of the channel state is found as

$$f_h(h)=\frac{\eta_s^2\exp(-\sigma_0^2/2)h_{af1}F_1\left(-\frac{1}{2},\frac{1}{2};\frac{\sigma_0^2}{2}\right)}{2\pi q_H\Gamma(k)}$$
$$\times\int_{-\pi}^{\pi}\frac{h^{\eta_s^2\xi(\varphi)-1}\theta^{-\eta_s^2\xi(\varphi)}}{A_0^{\eta_s^2\xi(\varphi)}h_{al}^{\eta_s^2\xi(\varphi)}}G_{1,2}^{2,0}\left(\frac{h}{\theta A_0h_{al}}\Big|_{0,k-\eta_s^2\xi(\varphi)}^{1}\right)d\varphi. \quad (39)$$

Inserting (39) into (32), the CDF of the channel state for Gamma distributed channel model is

$$F_h(h)=\frac{\eta_s^2\exp(-\sigma_0^2/2)h_{af1}F_1\left(-\frac{1}{2},\frac{1}{2};\frac{\sigma_0^2}{2}\right)}{2\pi q_H\Gamma(k)}$$
$$\times\int_{-\pi}^{\pi}\frac{\theta^{-\eta_s^2\xi(\varphi)}}{A_0^{\eta_s^2\xi(\varphi)}h_{al}^{\eta_s^2\xi(\varphi)}}d\varphi$$
$$\times\int_0^h x^{\eta_s^2\xi(\varphi)-1}G_{1,2}^{2,0}\left(\frac{x}{\theta A_0h_{al}}\Big|_{0,k-\eta_s^2\xi(\varphi)}^{1}\right)dx. \quad (40)$$

To solve x dependent integration in (40), we will use (26) of [25]. The, the CDF will be

$$F_h(h)=\frac{\eta_s^2\exp(-\sigma_0^2/2)h_{af1}F_1\left(-\frac{1}{2},\frac{1}{2};\frac{\sigma_0^2}{2}\right)}{2\pi q_H\Gamma(k)}\int_{-\pi}^{\pi}\frac{\theta^{-\eta_s^2\xi(\varphi)}}{A_0^{\eta_s^2\xi(\varphi)}}$$
$$\times\frac{h^{\eta_s^2\xi(\varphi)}}{h_{al}^{\eta_s^2\xi(\varphi)}}G_{2,3}^{2,1}\left(\frac{h}{\theta A_0h_{al}}\Big|_{0,k-\eta_s^2\xi(\varphi),-\eta_s^2\xi(\varphi)}^{1-\eta_s^2\xi(\varphi),1}\right)d\varphi. \quad (41)$$

Using the relationship given in (35), the outage probability is

$$P_{out}=\frac{\eta_s^2\exp(-\sigma_0^2/2)h_{af1}F_1\left(-\frac{1}{2},\frac{1}{2};\frac{\sigma_0^2}{2}\right)}{2\pi q_H\Gamma(k)}\int_{-\pi}^{\pi}\frac{\theta^{-\eta_s^2\xi(\varphi)}}{A_0^{\eta_s^2\xi(\varphi)}}$$
$$\times\frac{h_{th}^{\eta_s^2\xi(\varphi)}}{h_{al}^{\eta_s^2\xi(\varphi)}}G_{2,3}^{2,1}\left(\frac{h_{th}}{\theta A_0h_{al}}\Big|_{0,k-\eta_s^2\xi(\varphi),-\eta_s^2\xi(\varphi)}^{1-\eta_s^2\xi(\varphi),1}\right)d\varphi. \quad (42)$$

For the special case $q_H=1$, the closed-form expression of outage probability in (42) becomes

$$P_{out}=\frac{\eta_s^2\exp(-\sigma_0^2/2)h_{af1}F_1\left(-\frac{1}{2},\frac{1}{2};\frac{\sigma_0^2}{2}\right)}{\Gamma(k)}\frac{\theta^{-\eta_s^2}h_{th}^{\eta_s^2}}{A_0^{\eta_s^2}h_{al}^{\eta_s^2}}$$
$$\times G_{2,3}^{2,1}\left(\frac{h_{th}}{\theta A_0h_{al}}\Big|_{0,k-\eta_s^2,-\eta_s^2}^{1-\eta_s^2,1}\right). \quad (43)$$

C. Exponentiated Weibull Distributed Channel Model

Inserting (19) and (25) into (29), we find the conditioned PDF of h_{ag} as

$$f_{h_{ag}|\theta_d}(h_{ag})=\frac{\eta_s^2\cos(\theta_d)}{2\pi q_H}\frac{\alpha\beta}{\eta^\beta}\int_{-\pi}^{\pi}\frac{h_{ag}^{\eta_s^2\xi(\varphi)-1}}{A_0^{\eta_s^2\xi(\varphi)}h_{al}^{\eta_s^2\xi(\varphi)}}d\varphi$$
$$\times\int_{\frac{h_{ag}}{A_0h_{al}}}^{\infty}h_{at}^{\beta-\eta_s^2\xi(\varphi)-1}\exp\left[-\left(\frac{h_{at}}{\eta}\right)^\beta\right]$$
$$\times\left\{1-\exp\left[-\left(\frac{h_{at}}{\eta}\right)^\beta\right]\right\}^{\alpha-1}dh_{at}. \quad (44)$$

Then, following the procedures given in Appendix-C (C.1)–(C.6), the PDF of the channel state is found as

$$f_h(h) = \frac{\eta_s^2 \alpha h_{af} \exp\left(-\frac{\sigma_0^2}{2}\right) {}_1F_1\left(-\frac{1}{2}, \frac{1}{2}; \frac{\sigma_0^2}{2}\right)}{2\pi q_H} \sum_{n=0}^{\infty} \frac{(-1)^n \Gamma(\alpha)}{n! \Gamma(\alpha - n)} \times \int_{-\pi}^{\pi} \frac{h^{\eta_s^2 \xi(\varphi) - 1}}{A_0^{\eta_s^2 \xi(\varphi)} h_{al}^{\eta_s^2 \xi(\varphi)} \eta^{\eta_s^2 \xi(\varphi)} (1+n)^{(\beta - \eta_s^2 \xi(\varphi))/\beta}} \times G_{1,2}^{2,0}\left(\frac{(1+n) h^{\beta}}{\eta^{\beta} A_0^{\beta} h_{al}^{\beta}} \Big|_{0, \frac{(\beta - \eta_s^2 \xi(\varphi))}{\beta}}^{1} \right) d\varphi. \tag{45}$$

Using (32), the CDF of exponentiated Weibull distributed channel is

$$F_h(h) = \frac{\eta_s^2 \alpha h_{af} \exp\left(-\frac{\sigma_0^2}{2}\right) {}_1F_1\left(-\frac{1}{2}, \frac{1}{2}; \frac{\sigma_0^2}{2}\right)}{2\pi q_H} \sum_{n=0}^{\infty} \frac{(-1)^n \Gamma(\alpha)}{n! \Gamma(\alpha - n)} \times \int_{-\pi}^{\pi} \frac{1}{A_0^{\eta_s^2 \xi(\varphi)} h_{al}^{\eta_s^2 \xi(\varphi)} \eta^{\eta_s^2 \xi(\varphi)} (1+n)^{(\beta - \eta_s^2 \xi(\varphi))/\beta}} d\varphi \times \int_0^{h} x^{\eta_s^2 \xi(\varphi) - 1} G_{1,2}^{2,0}\left(\frac{(1+n) x^{\beta}}{\eta^{\beta} A_0^{\beta} h_{al}^{\beta}} \Big|_{0, \frac{(\beta - \eta_s^2 \xi(\varphi))}{\beta}}^{1} \right) dx. \tag{46}$$

To solve x dependent integration in (32), first changing the variable as $t = x^{\beta}$ and then using (26) of [25]

$$F_h(h) = \frac{\eta_s^2 \alpha h_{af} \exp\left(-\frac{\sigma_0^2}{2}\right) {}_1F_1\left(-\frac{1}{2}, \frac{1}{2}; \frac{\sigma_0^2}{2}\right)}{2\pi q_H \beta} \sum_{n=0}^{\infty} \frac{(-1)^n \Gamma(\alpha)}{n! \Gamma(\alpha - n)} \times \int_{-\pi}^{\pi} \frac{h^{\eta_s^2 \xi(\varphi)}}{A_0^{\eta_s^2 \xi(\varphi)} h_{al}^{\eta_s^2 \xi(\varphi)} \eta^{\eta_s^2 \xi(\varphi)} (1+n)^{(\beta - \eta_s^2 \xi(\varphi))/\beta}} \times G_{2,3}^{2,1}\left(\frac{(1+n) h^{\beta}}{\eta^{\beta} A_0^{\beta} h_{al}^{\beta}} \Big|_{0, \frac{(\beta - \eta_s^2 \xi(\varphi))}{\beta}, -\frac{\eta_s^2 \xi(\varphi)}{\beta}}^{1 - \frac{\eta_s^2 \xi(\varphi)}{\beta}, 1} \right) d\varphi. \tag{47}$$

Then, the outage probability will be obtained as

$$P_{out} = \frac{\eta_s^2 \alpha h_{af} \exp\left(-\frac{\sigma_0^2}{2}\right) {}_1F_1\left(-\frac{1}{2}, \frac{1}{2}; \frac{\sigma_0^2}{2}\right)}{2\pi q_H \beta} \sum_{n=0}^{\infty} \frac{(-1)^n \Gamma(\alpha)}{n! \Gamma(\alpha - n)} \times \int_{-\pi}^{\pi} \frac{h_{th}^{\eta_s^2 \xi(\varphi)}}{A_0^{\eta_s^2 \xi(\varphi)} h_{al}^{\eta_s^2 \xi(\varphi)} \eta^{\eta_s^2 \xi(\varphi)} (1+n)^{(\beta - \eta_s^2 \xi(\varphi))/\beta}} \times G_{2,3}^{2,1}\left(\frac{(1+n) h_{th}^{\beta}}{\eta^{\beta} A_0^{\beta} h_{al}^{\beta}} \Big|_{0, \frac{(\beta - \eta_s^2 \xi(\varphi))}{\beta}, -\frac{\eta_s^2 \xi(\varphi)}{\beta}}^{1 - \frac{\eta_s^2 \xi(\varphi)}{\beta}, 1} \right) d\varphi. \tag{48}$$

For the special case $q_H = 1$, the closed-form expression of outage probability for exponentiated Weibull distribution will be

$$P_{out} = \frac{\eta_s^2 \alpha h_{af} \exp\left(-\frac{\sigma_0^2}{2}\right) {}_1F_1\left(-\frac{1}{2}, \frac{1}{2}; \frac{\sigma_0^2}{2}\right)}{\beta} \times \sum_{n=0}^{\infty} \frac{(-1)^n \Gamma(\alpha)}{n! \Gamma(\alpha - n)} \frac{h_{th}^{\eta_s^2}}{A_0^{\eta_s^2} h_{al}^{\eta_s^2} \eta^{\eta_s^2} (1+n)^{(\beta - \eta_s^2)/\beta}} \times G_{2,3}^{2,1}\left(\frac{(1+n) h_{th}^{\beta}}{\eta^{\beta} A_0^{\beta} h_{al}^{\beta}} \Big|_{0, \frac{(\beta - \eta_s^2)}{\beta}, -\frac{\eta_s^2}{\beta}}^{1 - \frac{\eta_s^2}{\beta}, 1} \right). \tag{49}$$

It can be seen from (36), (42) and (48) that, showing the outage probabilities for Lognormal, Gamma, and exponentiated Weibull distributions, an integral term depending on the polar angle φ brings a complexity and it is not possible to solve analytically. The results are obtained numerically by evaluating φ dependent integral. Also, a series with infinite summation is involved in the equations related to the exponentiated Weibull distribution resulting from expansion of the Newton's generalized-binomial theorem. We verified that the series converges in the first 10 terms or more terms. However, we took into account 20 terms in our numerical computation to make sure that we present the exact result of the converging sum.

TABLE V
FIXED PARAMETERS

Symbol	Value
λ	1550 nm
ζ_{GH}	20 °
ζ_{GS}	30 °
H_H	20 km
H_S	36500 km
h_0	10 m
V	10 km
D_G	5 cm (GH link)
D_G	10 cm (GS link)
D_G	10 cm (HS link)
W_0	2 cm
F_0	∞
w	21 m/s
A	1.7×10^{-13} m$^{-2/3}$
q_H	0.9
σ_s	$5 \times r_a$
σ_z	$q_H \times \sigma_s$
σ_0	15 mrad
ω_b	$10 \times r_a$
η_s	$\omega_e/(2\sigma_s)$
LWC	3.28×10^{-4} g.m^{-3}
CNC	0.5 cm^{-3}

V. RESULTS AND DISCUSSION

In this section, the analytical results obtained from the derivated expressions are presented depending on the various parameters and conditions. The values of used parameters are chosen as listed in Table V. Any difference in the parameter from those in the table are mentioned in either figure captions or in

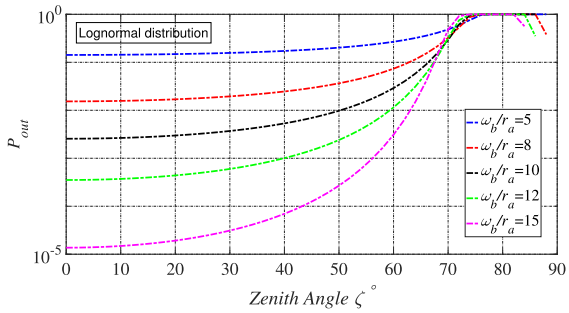

Fig. 2. The probability of outage for the FSO downlink between GS and HAPS as a function of zenith angle for various ω_b/r_a values.

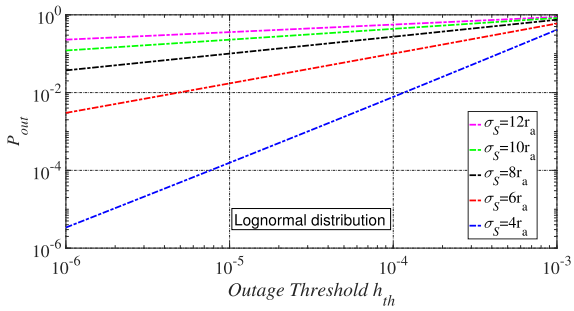

Fig. 3. The outage probability of the ground to HAPS FSO downlink versus the altitude for different values of σ_S.

the plots. Also, the used channel model for turbulence-induced fading is given on each plot. The performance of various links (slant path and horizontal) are illustrated and evaluated in terms of outage probability. Moreover, the comparisons of direct and HAPS assisted ground to GEO satellite links and, channel models are shown.

A. Ground to HAPS Communication Link

In Fig. 2, the probability of outage for a downlink between ground to HAPS is depicted versus zenith angle ζ and, ω_b/r_a. As it can be observed from Fig. 2 that the probability of outage degrades with the increase of the zenith angle and keeping the zenith angle smaller yields better performance. For example, the outage probability varies from $P_{out} \approx 3.5 \times 10^{-4}$ to $P_{out} \approx 1.1 \times 10^{-2}$ when the zenith angle varies from $\zeta = 0^\circ$ to $\zeta = 60^\circ$. In [18], it is expressed that the atmospheric turbulence remains in weak regime for slant path link while the zenith angle is $\zeta < 45^\circ$ or $\zeta < 60^\circ$. We also observe similar variation in Fig. 2. When zenith angle exceeds $\approx \zeta > 70^\circ$, the outage probability takes its highest values and the performance of the communication link becomes worst. We also observe some reversed decrease trends in outage probability when $\zeta > 80^\circ$ which is the result of scintillation saturation in the strong turbulence regime. Again, we see from Fig. 2 that the outage probability takes smaller values when the beam waist is on the higher order of receiver aperture radius. The outage probability of downlink between ground to HAPS for zenith angle $\zeta = 50^\circ$ drops from $P_{out} \approx 2 \times 10^{-1}$ to $P_{out} \approx 2.7 \times 10^{-4}$ when the ratio of beam waist to aperture radius increases from $\omega_b/r_a = 5$ to $\omega_b/r_a = 15$. This is due to the increasing possibility of collecting optical beam by the receiver aperture with the increase of beam waist that occurs for the long range of the ground to HAPS communication link. This shows that the performance of FSO communication link can be improved significantly with the appropriate level of the beam waist.

Fig. 3 demonstrates the variation of the outage probability depending on the outage threshold for various displacement values. The outage probability increases with increasing of the channel state threshold for a FSO downlink. Keeping the beam deviation as $\sigma_S = 6 \times r_a$ in Fig. 3, the outage probability rises from $P_{out} \approx 3 \times 10^{-3}$ to $P_{out} \approx 5.9 \times 10^{-1}$ when the threshold of the channel state increases from $h_{th} = 1 \times 10^{-6}$ to $h_{th} = 1 \times 10^{-3}$. The performance degrading effect of the beam displacement is also clearly seen in Fig. 3. Increasing σ_S from $\sigma_S = 4 \times r_a$ to $\sigma_S = 12 \times r_a$ causes significant performance degradation yielding outage probabilities from $P_{out} \approx 1.5 \times 10^{-4}$ to $P_{out} \approx 3.5 \times 10^{-1}$ while the outage threshold is kept as $h_{th} = 1 \times 10^{-5}$. Figs. 4 and 5 illustrate the outage performance of an FSO uplink between ground to HAPS using the same parameters given in Figs. 2 and 3, respectively. Similar to downlink, the performance degradation with the larger zenith angle, channel state threshold, beam displacement and smaller ω_b/r_a is observed for uplink communication. The benefit of smaller zenith angle, beam displacement and larger beam waist is clearly seen from Figs. 2–5 for both downlink and uplink.

We note that although the downlink and uplink yield similar performances (e.g., Figs. 2–4, Figs. 3–5), the outage probability of downlink remains lower very slightly. This slight difference

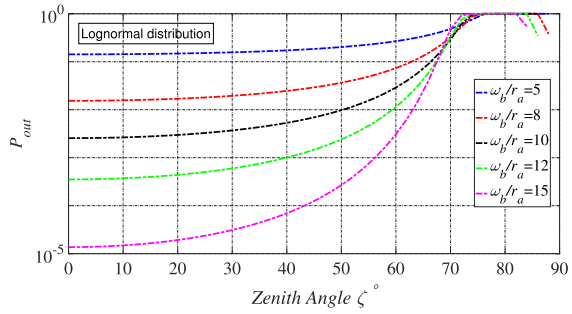

Fig. 4. The probability of outage for the ground to HAPS FSO uplink versus the zenith angle for various values of ω_b/r_a.

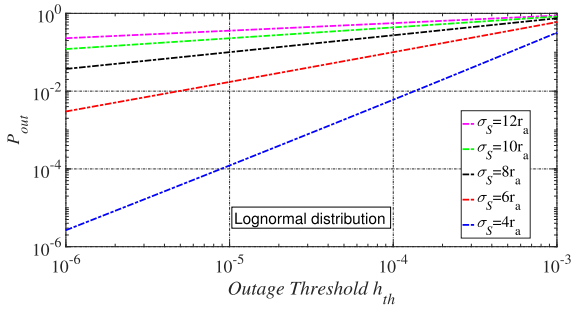

Fig. 5. The outage probability of the ground to HAPS FSO uplink versus the altitude for different values of σ_S.

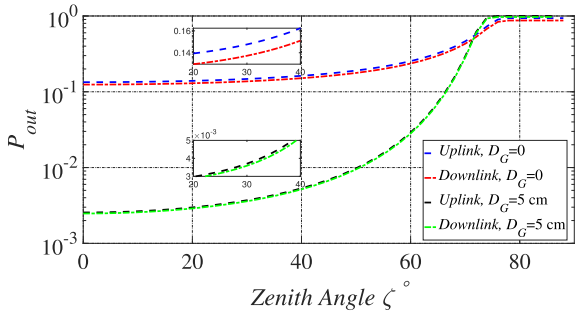

Fig. 6. The comparison of outage probability of the downlink and uplink ground to HAPS FSO link versus zenith angle for different receiver aperture diameters.

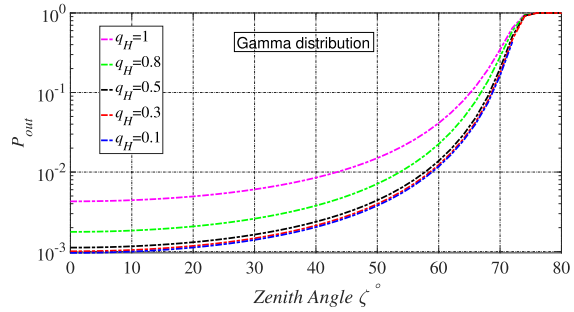

Fig. 7. The probability of outage for the ground to satellite downlink versus the zenith angle and various q_H values.

tends to increase for higher turbulence effects. To reflect the difference between outage performances of downlink and uplink, the comparison of uplink and downlink is given in Fig. 6 for two different receiver aperture diameter values ($D_G = 5$ cm and $D_G = 0$ point receiver). It is seen from Fig. 6 that the outage performance of downlink maintains at lower level than uplink for all cases. The reason why the performance of downlink is better may be that the optical beam encounters the higher turbulence effect in the last phase of its propagation (optical beam first propagates and then is distorted in short duration) while this happens in the initial phase for uplink (optical beam is distorted and then distorted beam propagates). However, the level of difference between the outage probabilities of downlink and uplink can be assumed to be negligible when receiver with large aperture is used. It is also observed from Fig. 6 that outage performances of downlink and uplink are very close to each other for larger aperture sizes and the difference between downlink and uplink performances becomes more visible when receiver aperture size takes smaller sizes. This shows that the use of aperture average is also minimizing the difference in performance between uplink and downlink scenarios.

B. Ground to Satellite Communication Link

We evaluate the performance of FSO downlink and uplink communication between ground to GEO satellite for different parameters in Figs. 7–10. Fig. 7 shows the probability of outage variation for the FSO downlink communication versus zenith angle forvarious q_H values. When the beam deviations in both

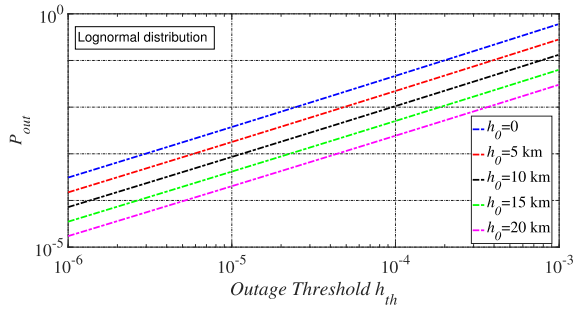

Fig. 8. The probability of outage for the FSO downlink between ground station and satellite versus the outage threshold for various values of h_0.

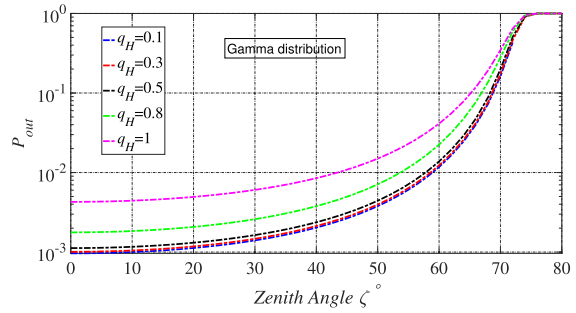

Fig. 9. The probability of outage for the ground to satellite uplink versus the zenith angle and various values of q_H.

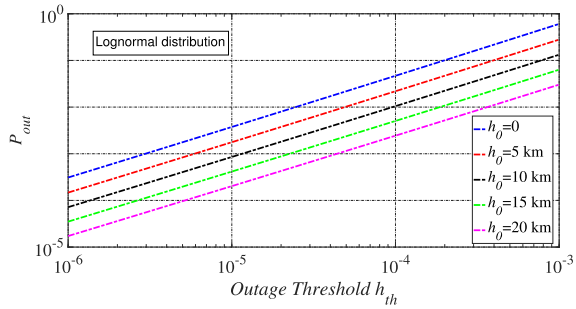

Fig. 10. The outage probability of the ground to satellite uplink versus the channel state threshold for different values of h_0.

directions are identical ($q_H = 1$), the outage probability starts from $P_{out} \approx 4.3 \times 10^{-4}$ and reachs to $P_{out} \approx 3.5 \times 10^{-1}$ with the rise of the zenith angle from $\zeta = 0°$ to $\zeta = 70°$. When the zenith angle exceeds the value of $\zeta \approx 70°$, the link is almost lost and the outage performance takes the highest values. It can be inferred from Fig. 7 the FSO downlink benefits from the asymmetrical behaviour of the beam deviations while $q_H < 1$. This is due to the σ_Z remains smaller than σ_S and leads to a decrease in the probability of outage compared with the symmetrical case $\sigma_Z = \sigma_S$. For example, keeping the zenith angle as $\zeta = 30°$, the probability of outage changes from $P_{out} \approx 1.4 \times 10^{-3}$ to $P_{out} \approx 6 \times 10^{-3}$ when the beam deviatons change from Hoyt distribution ($q_H = 0.1$) to Rayleigh distribution ($q_H = 1$). In Fig. 8, a monotonic logarithmic increase in the outage probability is seen depending on the increase in the threshold of the channel state. The impact of the height of the GS is also plotted in Fig. 8. When ground station is deployed at the ground level

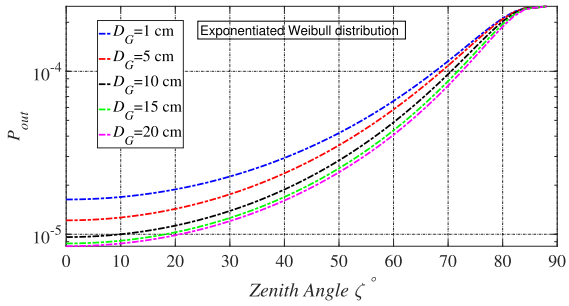

Fig. 11. The outage probability of the HAPS to satellite downlink versus of zenith angle for various receiver aperture diameter values.

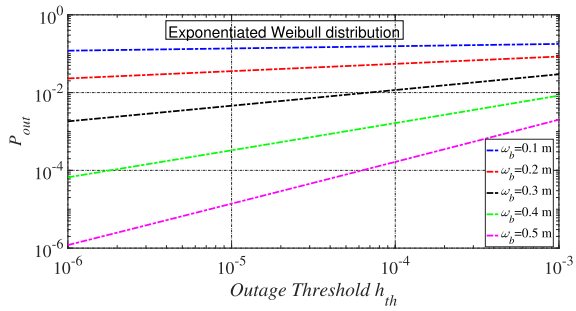

Fig. 12. The outage probability of the HAPS to satellite uplink versus the outage threshold for different values of ω_b.

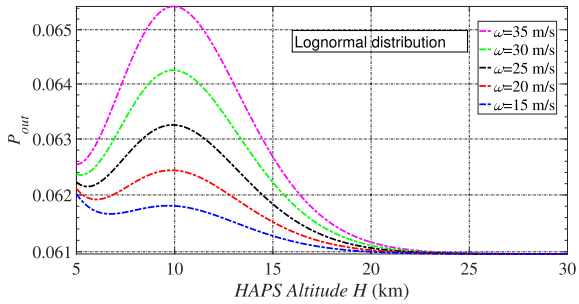

Fig. 13. The outage probability of a HAPS to HAPS horizontal link versus altitude for various wind speed values.

$h_0 = 0$ the outage probability takes the highest level. However, if the communication link becomes low altitude platforms (LAPS) or HAPS assisted starting from $h_0 = 5$ km then, the performance of communication system improves gradually with the increase of the height of the lower station. Fixing the threshold of the channel state to $h_{th} = 1 \times 10^{-5}$, the outage probabiliy gets smaller and takes the values of $P_{out} \approx 3.7 \times 10^{-3}$, $P_{out} \approx 8.6 \times 10^{-4}$ and $P_{out} \approx 2 \times 10^{-4}$ with the increase of the height of the GS as $h_0 = 0$, $h_0 = 10$ km (HAPS assisted) and $h_0 = 20$ km (HAPS assisted), respectively.

In Fig. 9, we observe a degradation in the probability of outage with the rise of the zenith angle for FSO uplink similar to the variation for downlink given in Fig. 7. For Hoyt distributed deviation case $q_H = 0.1$, the performance of the uplink FSO communication system degrades by taking the values of $P_{out} \approx 4.2 \times 10^{-3}$ and $P_{out} \approx 3.5 \times 10^{-1}$ when zenith angle is $\zeta = 0°$ and $\zeta = 70°$. The decrease in the ratio of vertical and horizontal deviations yields an improvement in the performance of the uplink FSO communication systems as it can be seen from Fig. 9.

The benefit of using LAPS and HAPS compared to the ground based uplink can be inferred from Fig. 10 for uplink FSO communication. The outage probability falls from $P_{out} \approx 4.7 \times 10^{-2}$ to $P_{out} \approx 2.4 \times 10^{-3}$ when the height of the lower station increases from $h_0 = 0$ (ground level) to $h_0 = 20$ km (HAPS assisted) for threshold of the channel state as $h_{th} = 1 \times 10^{-4}$. The results for both downlink and uplink FSO communication show that keeping the lower station as much as higher altitude will lead of avoidance of the atmospheric attenuation and turbulence effects.

C. HAPS to Satellite Communication Link

Fig. 11 reflects the probability of outage variation with the zenith angle for different values of the receiver aperture diameter. The figures above show that the probability of outage for FSO downlink decreases with small zenith angle values.

It is also seen that increasing the receiver aperture size causes performance improvement for FSO link. For example, the outage probability decreases from $P_{out} \approx 1.7 \times 10^{-5}$ to $P_{out} \approx 8.7 \times 10^{-6}$ with the increase of receiver aperture diameter from $D_G = 1$ cm to $D_G = 20$ cm while the zenith angle is fixed to $\zeta = 20°$. The increase in the receiver aperture diameter starts to change the outage performance slightly because of the larger receiver collects all the intensity and saturates showing that the receiver aperture size should be optimized to provide the optimum performance improvement with the aperture averaging. The performance improvement with enlargement of the receiver aperture diameter becomes smaller when zenith angle increases. However, it is observed that aperture averaging remains a useful technique in terms of mitigating the degradation effects caused by turbulence.

In Fig. 12, the radius of receiver aperture is fixed to $r_a = 5$ cm and only the beam waist is changed to observe the performance of HAPS to satellite FSO uplink. Keeping the outage threshold as $h_{th} = 1 \times 10^{-5}$ then changing the beam waist from $\omega_b = 0.1$ m to $\omega_b = 0.5$ m yields a remarkable performance improvement by pulling down the outage probability from $P_{out} \approx 1.3 \times 10^{-1}$ to $P_{out} \approx 1.4 \times 10^{-5}$.

D. HAPS to HAPS Communication Link

The ground to satellite communication link may be provided via first ground to HAPS later HAPS to HAPS network and the last HAPS to satellite links. That's why we show the performance results of the horizontal FSO link in the following Figs. 13 and 14. In Fig. 13, it is observed that the probability of outage rises with the increase of altitude up to a certain level (here $H \approx 10$ km) and then outage probability starts to decrease with the increase of altitude until taking almost its constant value $H \approx 20$ km. The outage probability maintains its almost constant trend after $H \approx 20$ km altitude. Another parameter, the wind speed, shows its influence on the outage probability until $H \approx 20$ km the outage probability almost does not change with the wind speed change.

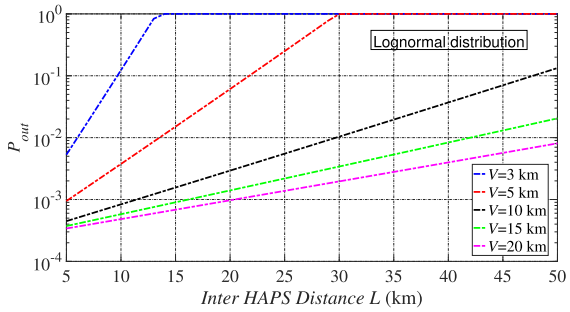

Fig. 14. The outage probability of a HAPS to HAPS horizontal link versus link length for different values of the visibility.

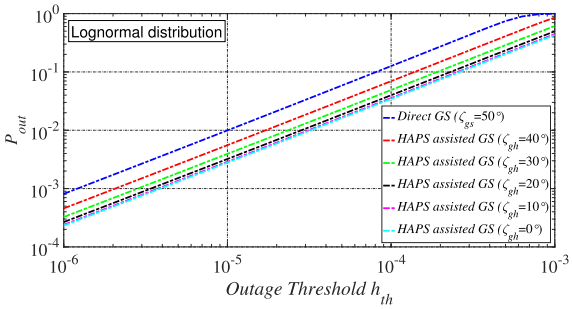

Fig. 15. The the comparison of outage probabilities for direct ground-to-satellite and HAPS assisted ground-to-satellite links versus channel state threshold.

In Fig. 14, the performance of a horizontal FSO link is plotted versus of link distance and the visibility parameter. The performance degradation with the link distance is seen as expected. The high impact of the visibility that depends on the atmospheric conditions is also observed from Fig. 14. Outage probability takes the worst values at $L \approx 14\,\text{km}$ and $L \approx 30\,\text{km}$ for the values of visibility as $V = 3\,\text{km}$ and $V = 5\,\text{km}$, respectively. Given that the $V = 1.9\,\text{km}$ for thin foggy weather in Table II, the drastic performance degradation of the FSO links with fog still remains challenging.

E. Comparison of Direct Link Versus Relayed Link

The outage probability of HAPS assisted ground to satellite link with decoding and forwarding capabilities at the HAPS can be found as

$$P_{out}^{GS}(h \le h_{th}) = 1 - \left\{1 - P_{out}^{GH}(h \le h_{th})\right\} \times \left\{1 - P_{out}^{HS}(h \le h_{th})\right\}, \quad (50)$$

where $P_{out}^{GH}(h \le h_{th})$ and $P_{out}^{HS}(h \le h_{th})$ are the outage probabilities of ground-to-HAPS and HAPS-to-satellite links.

To characterize the benefit of using HAPS relaying between ground to GEO satellite communications, the outage probability variation versus channel state threshold is given for various HAPS deployment configurations (depending on the zenith angle) in Fig. 15. Here, the zenith angle for ground to GEO satellite link is set to $\zeta_{GS} = 50^\circ$, the zenith angle for ground to HAPS ζ_{GH} is kept smaller than ζ_{GS} and the zenith angle for

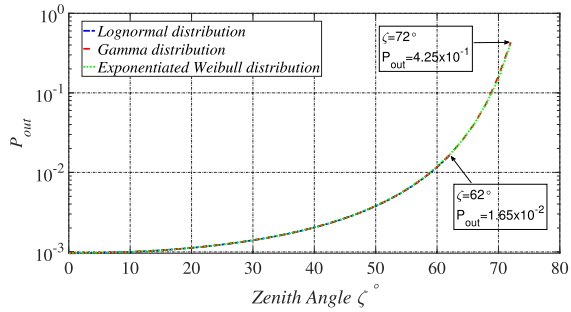

Fig. 16. Comparison of the Lognormal, Gamma and exponentiated Weibull distributions for ground-to-satellite uplinks versus the zenith angle.

HAPS to satellite ζ_{HS} is calculated by using geometric relations depending on the ζ_{GH}, ζ_{GS} and altitudes. The receiver aperture diameter D_G values are chosen as 5 cm for ground to HAPS link, 10 cm for HAPS to satellite link and 10 cm for ground to satellite link. Keeping the outage threshold as $h_{th} = 1 \times 10^{-5}$, the probability of outage takes the value of $P_{out} \approx 1 \times 10^{-2}$. When HAPS relaying is used, the outage probability values become $P_{out} \approx 5.5 \times 10^{-3}$, $P_{out} \approx 3.2 \times 10^{-3}$ and $P_{out} \approx 2.7 \times 10^{-3}$ for zenith angles $\zeta_{GH} = 40^\circ$, $\zeta_{GH} = 20^\circ$ and $\zeta_{GH} = 0^\circ$. It is obvious that the best performance can be obtained for the vertical alignment of the GS and HAPS ($\zeta_{GH} = 0^\circ$). Finally, to verify the accuracy of our derivations and compare the turbulent channel models, we present the comparison of Lognormal, Gamma and exponentiated Weibull distributions in Fig. 16. We see that three models match perfectly. The important point is the Lognormal distribution gives the results until zenith angle reaches $\zeta = 62^\circ$ then it does not perform calculations. This behavior is consistent with the Lognormal distribution that yields effective results when weak atmospheric turbulence conditions are available. The Gamma and exponentiated Weibull distributions yield the results in moderate to strong turbulence regimes and then they lose their sensitivity when zenith angle exceeds $\zeta = 72^\circ$ which corresponds to the boundary of saturated strong turbulence regime.

Results show that the selection of appropriate channel model should be based on the turbulence strength rather than application type (HAPS to HAPS, ground to HAPS, HAPS to satellite). Lognormal, Gamma and exponentiated Weibull channel models can be used for the performance analysis in weak turbulence conditions. When strong turbulence conditions are available, Lognormal tends not to perform then Gamma and exponentiated Weibull models remain as accurate solutions providing almost the same performances. For a slant path communication link having small zenith angle, Lognormal, Gamma and exponentiated Weibull models can be used with similar performances. However, Lognormal model do not provide any results when zenith angle is high due to strong turbulence effect.

In terms of application types, HAPS to satellite communication link, that is exposed almost no turbulence effect, can be modeled by Lognormal, Gamma and exponentiated Weibull distributed channel models. However, a horizontal or slant path link experiencing the turbulence conditions in troposphere and

lower stratosphere layers (approximately < 20 km altitude), including ground to HAPS, HAPS to HAPS and ground to satellite communication links, need to be modeled carefully by taking into account the strength of the turbulence.

VI. Future Investigations

In this study, the performance of integrated ground-air-space communication links is presented for single-input single-output (SISO) systems. The benefit of using HAPS as relaying is seen from the obtained results up to a certain level. To overcome turbulence-induced degradation effects and increase the performance of integrated ground-air-space based communication systems, mitigation techniques (spatial diversity techniques and adaptive optics correction methods are analyzed extensively for various applications) can be other considerable solutions in terms of performance improvement. We have already investigated the performance improvement with adaptive optics correction methods for ground to HAPS communication links in Gamma-Gamma distributed turbulent channel model [12]. Diversity techniques, using multiple apertures at transmitter and/or receiver side, are worthy of investigation in terms of additional improvement in the performance of HAPS assisted applications. The power gain and reduced scintillation with the help of statistically independent multiple apertures for single-input multiple-output (SIMO), multiple-input single-output (MISO) and MIMO systems have the potential to be the extension of this work.

In addition, the inclusion of the round-trip time (RTT) latency is seen as an important figure of merit to ensure the continuity of the stream of data, especially comparing the cases of HAPS relaying ground to satellite communication and direct ground to satellite link. Including RTT latency is another investigation parameter to characterize the performance of HAPS assisted communication links.

VII. Conclusion

We investigated the performance of integrated ground-air-space FSO communication links between ground and GEO satellite, ground and HAPS, HAPS and HAPS and, HAPS and satellite. The joint effect of atmospheric attanuation, pointing error, AOA fluctuations and atmospheric turbulence is included in proposed model. Three models, namely Lognormal, Gamma and exponentiated Weibull distributions, are used for atmospheric turbulence characterization. Closed-form expressions for channel PDF, CDF and probability of outage are extracted using Lognormal, Gamma and exponentiated Weibull distributions separately. The pointing error effect is modeled by Hoyt distribution. The performance of slant path and horizontal links is affected from beam waist, beam deviation, channel state, the ratio of vertical and horizontal deviations, the altitude of upper stations, the height of lower stations, receiver aperture diameter, wind speed and zenith angle. The HAPS assisted ground to satellite link yields better performance than the direct ground to satellite link. The best performance is obtained with HAPS assisted link with zenith angle $\zeta_{GH} = 0^\circ$ between ground to HAPS. The results given in this study may be useful for characterizing different slant path and horizontal FSO links for integrated ground-air-space applications operating in various turbulence environment.

Appendix A
Lognormal Channel Model Derivations

We can expand the exponential term in (30) as

$$\exp\left[-\frac{\ln^2(h_{at})+\sigma_l^2\ln(h_{at})+\sigma_l^4/4}{2\sigma_l^2}\right] = \exp\left[-\frac{\ln^2(h_{at})}{2\sigma_l^2}\right]\exp\left[-0.5\ln(h_{at})\right]\exp(-\sigma_l^2/8). \tag{A.1}$$

Then, (30) becomes

$$f_{h_{ag}|\theta_d}(h_{ag}) = \frac{\eta_s^2\cos(\theta_d)\exp(-\sigma_l^2/8)}{2\pi q_H\sqrt{2\pi\sigma_l^2}}\int_{-\pi}^{\pi}\frac{h_{ag}^{\eta_s^2\xi(\varphi)-1}}{(A_0h_{al})^{\eta_s^2\xi(\varphi)}}d\varphi \times\int_{\frac{h_{ag}}{A_0h_{al}}}^{\infty}\frac{1}{h_{at}^{\eta_s^2\xi(\varphi)+3/2}}\exp\left[-\frac{\ln^2(h_{at})}{2\sigma_l^2}\right]dh_{at}. \tag{A.2}$$

Changing variable as $\delta = \ln(h_{at})/\sqrt{(2\sigma_l^2)}$, (A.2) becomes

$$f_{h_{ag}|\theta_d}(h_{ag}) = \frac{\eta_s^2\cos(\theta_d)\exp(-\sigma_l^2/8)}{2\pi\sqrt{\pi}q_H}\int_{-\pi}^{\pi}\frac{h_{ag}^{\eta_s^2\xi(\varphi)-1}}{(A_0h_{al})^{\eta_s^2\xi(\varphi)}}d\varphi \times\int_{\frac{\ln\left(\frac{h_{ag}}{A_0h_{al}}\right)}{\sqrt{2\sigma_l^2}}}^{\infty}\exp\left[-\delta^2-\sqrt{2\sigma_l^2}(\eta_s^2\xi(\varphi)+\frac{1}{2})\delta\right]d\delta. \tag{A.3}$$

We solve the integration in (A.3) by using the (3.322-1) of [26] that is given by

$$\int_u^{\infty}\exp\left(-x^2-2ax\right)dx = \frac{\sqrt{\pi}}{2}e^{a^2}\left[1-\mathrm{erf}(a+u)\right]. \tag{A.4}$$

Applying (A.4) to (A.3),

$$f_{h_{ag}|\theta_d}(h_{ag}) = \frac{\eta_s^2\cos(\theta_d)\exp(-\sigma_l^2/8)}{4\pi q_H}\int_{-\pi}^{\pi}\frac{h_{ag}^{\eta_s^2\xi(\varphi)-1}}{A_0^{\eta_s^2\xi(\varphi)}h_{al}^{\eta_s^2\xi(\varphi)}}d\varphi \times\exp\left[\frac{\sigma_l^2(\eta_s^2\xi(\varphi)+1/2)^2}{2}\right] \times\left\{1-\mathrm{erf}\left[\frac{\ln\left(\frac{h_{ag}}{A_0h_{al}}\right)+\sigma_l^2(\eta_s^2\xi(\varphi)+\frac{1}{2})}{\sqrt{2\sigma_l^2}}\right]\right\}. \tag{A.5}$$

The PDF of the channel state is obtained by

$$f_h(h) = \int_0^{\infty}h_{af}f_{h_{ag}|\theta_d}(h)f_{\theta_d}(\theta_d)d\theta_d. \tag{A.6}$$

Considering $\theta_d \leq \theta_{FOV}$, and then substituting (A.5) and (27) into (A.6), yielding

$$f_h(h) = \frac{\eta_s^2 \exp(-\sigma_l^2/8)}{4\pi q_H \sigma_0^2} h_{af} \int_{-\pi}^{\pi} \frac{h^{\eta_s^2 \xi(\varphi)-1}}{A_0^{\eta_s^2\xi(\varphi)} h_{al}^{\eta_s^2\xi(\varphi)}} d\varphi \times \exp\left[\frac{\sigma_l^2(\eta_s^2\xi(\varphi)+1/2)^2}{2}\right] \times \left\{1 - \text{erf}\left[\frac{\ln\left(\frac{h_{ag}}{A_0 h_{al}}\right) + \sigma_l^2(\eta_s^2\xi(\varphi)+\frac{1}{2})}{\sqrt{2\sigma_l^2}}\right]\right\} \times \int_0^{\infty} \theta_d \exp\left(-\frac{\theta_d^2}{2\sigma_0^2}\right)\cos(\theta_d) d\theta_d. \quad \text{(A.7)}$$

To drive the integral part in (A.7) depending on the parameter θ_d, we will use (3.952-8) of [26] expressed by

$$\int_0^{\infty} x^{\mu-1} e^{-\beta x^2} \cos(ax) dx = \frac{1}{2}\beta^{-\mu/2}\Gamma\left(\frac{\mu}{2}\right) e^{-a^2/4\beta} \times {}_1F_1\left(\frac{1-\mu}{2}, \frac{1}{2}; \frac{a^2}{4\beta}\right), \quad \text{(A.8)}$$

where $a > 0$, $\text{Re}(\mu) > 0$, $\text{Re}(\beta) > 0$ and ${}_1F_1(.)$ is Hypergeometric function. We obtain the PDF of the channel as given in (31) by using (A.8) in (A.7).

Changing variable in (33) as $t = ln(\frac{x}{A_0 h_{al}})/\sqrt{2\sigma_l^2} + \sqrt{2\sigma_l^2}(\eta_s^2\xi(\varphi)+1/2)/2$, we obtain

$$F_h(h) = \frac{\eta_s^2 \exp(-\frac{\sigma_l^2}{8}) \exp(-\frac{\sigma_0^2}{2}) h_{af} \sqrt{2\sigma_l^2}\, {}_1F_1\left(-\frac{1}{2}, \frac{1}{2}; \frac{\sigma_0^2}{2}\right)}{4\pi q_H} \times \int_{-\pi}^{\pi} \exp\left[\frac{\sigma_l^2\left(\eta_s^2\xi(\varphi)+1/2\right)^2}{2} - \sqrt{2\sigma_l^2}\eta_s^2\xi(\varphi)\Delta_2\right] d\varphi \times \int_{-\infty}^{\Delta_1} \exp\left(\sqrt{2\sigma_l^2}\eta_s^2\xi(\varphi)t\right)[1 - \text{erf}(t)]\, dt, \quad \text{(A.9)}$$

where $\Delta_1 = ln(\frac{h}{A_0 h_{al}})/\sqrt{2\sigma_l^2} + \sqrt{2\sigma_l^2}(\eta_s^2\xi(\varphi)+1/2)/2$ and $\Delta_2 = \sqrt{2\sigma_l^2}(\eta_s^2\xi(\varphi)+1/2)/2$. We can expand (A.9) as

$$F_h(h) = \frac{\eta_s^2 \exp(-\frac{\sigma_l^2}{8}) \exp(-\frac{\sigma_0^2}{2}) h_{af} \sqrt{2\sigma_l^2}\, {}_1F_1\left(-\frac{1}{2}, \frac{1}{2}; \frac{\sigma_0^2}{2}\right)}{4\pi q_H} \times \int_{-\pi}^{\pi} \exp\left[\frac{\sigma_l^2\left(\eta_s^2\xi(\varphi)+1/2\right)^2}{2} - \sqrt{2\sigma_l^2}\eta_s^2\xi(\varphi)\Delta_2\right] d\varphi \times \left\{\int_{-\infty}^{\Delta_1} \exp\left(\sqrt{2\sigma_l^2}\eta_s^2\xi(\varphi)t\right) dt - \int_{-\infty}^{0} \exp\left(\sqrt{2\sigma_l^2}\eta_s^2\xi(\varphi)t\right)\text{erf}(t) dt - \int_0^{\Delta_1} \exp\left(\sqrt{2\sigma_l^2}\eta_s^2\xi(\varphi)t\right)\text{erf}(t) dt\right\}, \quad \text{(A.10)}$$

In (A.10), to change the limit of $-\infty$ to 0 integration using $-t = u$ variable conversion and utilizing the odd function property of erf as $\text{erf}(-u) = -\text{erf}(u)$, we obtain

$$F_h(h) = \frac{\eta_s^2 \exp(-\frac{\sigma_l^2}{8}) \exp(-\frac{\sigma_0^2}{2}) h_{af} \sqrt{2\sigma_l^2}\, {}_1F_1\left(-\frac{1}{2}, \frac{1}{2}; \frac{\sigma_0^2}{2}\right)}{4\pi q_H} \times \int_{-\pi}^{\pi} \exp\left[\frac{\sigma_l^2\left(\eta_s^2\xi(\varphi)+1/2\right)^2}{2} - \sqrt{2\sigma_l^2}\eta_s^2\xi(\varphi)\Delta_2\right] d\varphi \times \left\{\int_{-\infty}^{\Delta_1} \exp\left(\sqrt{2\sigma_l^2}\eta_s^2\xi(\varphi)t\right) dt + \int_0^{\infty} \exp\left(-\sqrt{2\sigma_l^2}\eta_s^2\xi(\varphi)u\right)\text{erf}(u) du - \int_0^{\Delta_1} \exp\left(\sqrt{2\sigma_l^2}\eta_s^2\xi(\varphi)t\right)\text{erf}(t) dt\right\}. \quad \text{(A.11)}$$

The u dependent integration in (A.11) is in the structure of Laplace transform that is given by $\mathcal{L}[f(t)](s) = \int_0^{\infty} f(t)e^{-st}dt$. The Laplace transform of erf is given as [27]

$$\mathcal{L}[\text{erf}(t)](z) = \frac{1}{z}\exp(z^2/4)\text{erfc}(z/2), Re(z) > 0. \quad \text{(A.12)}$$

Applying (A.12) to (A.11) and solving first two integrations (t and u dependent), we have

$$F_h(h) = \frac{\eta_s^2 \exp(-\frac{\sigma_l^2}{8}) \exp(-\frac{\sigma_0^2}{2}) h_{af} \sqrt{2\sigma_l^2}\, {}_1F_1\left(-\frac{1}{2}, \frac{1}{2}; \frac{\sigma_0^2}{2}\right)}{4\pi q_H} \times \int_{-\pi}^{\pi} \exp\left[\frac{\sigma_l^2\left(\eta_s^2\xi(\varphi)+1/2\right)^2}{2} - \sqrt{2\sigma_l^2}\eta_s^2\xi(\varphi)\Delta_2\right] d\varphi \times \left\{\frac{\exp\left(\sqrt{2\sigma_l^2}\eta_s^2\xi(\varphi)\Delta_1\right)}{\sqrt{2\sigma_l^2}\eta_s^2\xi(\varphi)} + \frac{\exp\left(\sigma_l^2\eta_s^4\xi^2(\varphi)/2\right)\text{erfc}\left(\sqrt{2\sigma_l^2}\eta_s^2\xi(\varphi)/2\right)}{\sqrt{2\sigma_l^2}\eta_s^2\xi(\varphi)} - \int_0^{\Delta_1} \exp\left(\sqrt{2\sigma_l^2}\eta_s^2\xi(\varphi)t\right)\text{erf}(t) dt\right\}. \quad \text{(A.13)}$$

The last term in (A.13) can be solved by using following relationship [28]

$$\int_0^b \exp(at)\text{erf}(t) dt = \frac{1}{a}\left\{\exp(a^2/4)\left[\text{erf}(a/2 - b) - \text{erf}(a/2)\right] + \exp(ab)\text{erf}(b)\right\}. \quad \text{(A.14)}$$

Applying (A.14) to (A.13), the CDF of channel state h for Lognormal distribution is found as given in (34).

APPENDIX B
GAMMA DISTRIBUTED CHANNEL MODEL DERIVATIONS

To solve h_{at} dependent integral in (38), we utilize (3.381-3) of [26] that is given as

$$\int_u^{\infty} x^{v-1}\exp(-\mu x) dx = \mu^{-v}\Gamma(v, \mu u), \quad \text{(B.1)}$$

where $u > 0$, $Re(\mu) > 0$, $\Gamma(s,t)$ is the incomplete Gamma function. Applying (B.1) to (38) and converting $\Gamma(s,t)$ to meijer-G function by using the relationship $\Gamma(a,z) = G_{1,2}^{2,0}(z\Big|_{0,a}^{1})$ given in (06.06.26.0005.01) of [27], we obtain

$$f_{h_{ag}|\theta_d}(h_{ag}) = \frac{\eta_s^2 \cos(\theta_d)}{2\pi q_H \Gamma(k)} \int_{-\pi}^{\pi} \frac{h_{ag}^{\eta_s^2\xi(\varphi)-1}\theta^{-\eta_s^2\xi(\varphi)}}{A_0^{\eta_s^2\xi(\varphi)} h_{al}^{\eta_s^2\xi(\varphi)}} \times G_{1,2}^{2,0}\left(\frac{h}{\theta A_0 h_{al}}\Bigg|_{0,k-\eta_s^2\xi(\varphi)}^{1}\right) d\varphi. \quad \text{(B.2)}$$

Inserting (B.2) into (A.6) and solving θ_d dependent integration by using the relationship given in (A.8), we reach the PDF of the channel state for Gamma distribution given in (39).

Appendix C
Exponentiated Weibull Channel Model Derivations

According to the Newton's generalized-binomial theorem

$$(1+z)^r = \sum_{n=0}^{\infty} \frac{\Gamma(r+1)}{n!\Gamma(r-n+1)} z^n. \quad \text{(C.1)}$$

The term $\{1-\exp[-(\frac{h_{at}}{\eta})^{\beta}]\}^{\alpha-1}$ in (44) can be expanded by using the Newton's General Binomial Theorem as

$$\left\{1-\exp\left[-\left(\frac{h_{at}}{\eta}\right)^{\beta}\right]\right\}^{\alpha-1} = \sum_{n=0}^{\infty} \frac{(-1)^n\Gamma(\alpha)}{n!\Gamma(\alpha-n)} \exp\left[-n\left(\frac{h_{at}}{\eta}\right)^{\beta}\right]. \quad \text{(C.2)}$$

Inserting (C.2) into (44), we find

$$f_{h_{ag}|\theta_d}(h_{ag}) = \frac{\eta_s^2\cos(\theta_d)\alpha\beta}{2\pi q_H \eta^{\beta}} \int_{-\pi}^{\pi} \frac{h_{ag}^{\eta_s^2\xi(\varphi)-1}}{A_0^{\eta_s^2\xi(\varphi)} h_{al}^{\eta_s^2\xi(\varphi)}} d\varphi \sum_{n=0}^{\infty} \frac{(-1)^n\Gamma(\alpha)}{n!\Gamma(\alpha-n)} \int_{\frac{h_{ag}}{A_0 h_{al}}}^{\infty} h_{at}^{\beta-\eta_s^2\xi(\varphi)-1} \times \exp\left[-\frac{(1+n)}{\eta^{\beta}} h_{at}^{\beta}\right] dh_{at}. \quad \text{(C.3)}$$

To solve h_{at} dependent integral in (C.3), we can use (3.381-9) of [26] that is given as

$$\int_u^{\infty} x^m \exp(-\mu x^n) dx = \frac{\Gamma(v, \mu u^n)}{n\mu^v}, \quad v = \frac{m+1}{n}, \quad Re(n) > 0, \; Re(\mu) > 0. \quad \text{(C.4)}$$

Applying (C.4) to (C.3) and then, using the relationship $\Gamma(a,z) = G_{1,2}^{2,0}(z\Big|_{0,a}^{1})$, we arrive at

$$f_{h_{ag}|\theta_d}(h_{ag}) = \frac{\eta_s^2\cos(\theta_d)\alpha}{2\pi q_H} \sum_{n=0}^{\infty} \frac{(-1)^n\Gamma(\alpha)}{n!\Gamma(\alpha-n)} \int_{-\pi}^{\pi} \frac{h_{ag}^{\eta_s^2\xi(\varphi)-1}}{(A_0 h_{al}\eta)^{\eta_s^2\xi(\varphi)}(1+n)^{(\beta-\eta_s^2\xi(\varphi))/\beta}} \times G_{1,2}^{2,0}\left(\frac{(1+n)h_{ag}^{\beta}}{\eta^{\beta}A_0^{\beta}h_{al}^{\beta}}\Bigg|_{0,\frac{(\beta-\eta_s^2\xi(\varphi))}{\beta}}^{1}\right) d\varphi. \quad \text{(C.5)}$$

To find the PDF of the link, we insert (C.5) into (A.6). Then,

$$f_h(h) = \frac{\eta_s^2\alpha h_{af}}{2\pi q_H \sigma_0^2} \sum_{n=0}^{\infty} \frac{(-1)^n\Gamma(\alpha)}{n!\Gamma(\alpha-n)} \int_{-\pi}^{\pi} \frac{h^{\eta_s^2\xi(\varphi)-1}}{(A_0 h_{al}\eta)^{\eta_s^2\xi(\varphi)}(1+n)^{(\beta-\eta_s^2\xi(\varphi))/\beta}} \times G_{1,2}^{2,0}\left(\frac{(1+n)h^{\beta}}{\eta^{\beta}A_0^{\beta}h_{al}^{\beta}}\Bigg|_{0,\frac{(\beta-\eta_s^2\xi(\varphi))}{\beta}}^{1}\right) d\varphi \int_0^{\infty} \theta_d \exp\left(-\frac{\theta_d^2}{2\sigma_0^2}\right)\cos(\theta_d) d\theta_d. \quad \text{(C.6)}$$

Solving θ_d dependent integral by using (A.8), we obtain the PDF of the channel for exponentiated Weibull distribution as given in (45).

References

[1] G. M. Djuknic, J. Freidenfelds, and Y. Okunev, "Establishing wireless communications services via high-altitude aeronautical platforms: A concept whose time has come?," *IEEE Commun. Mag.*, vol. 35, no. 9, pp. 128–135, Sep. 1997.

[2] M. Antonini, E. Cianca, A. D. Luise, M. Pratesi, and M. Ruggieri, "Stratospheric relay: Potentialities of new satellite-high altitude platforms integrated scenarios," in *Proc. IEEE Aerosp. Conf. Proc.*, 2003, pp. 3_1211–3_1219.

[3] S. Karapantazis and F. Pavlidou, "Broadband communications via high-altitude platforms: A survey," *IEEE Commun. Surveys Tuts.*, vol. 7, no. 1, pp. 2–31, Jan.–Mar. 2005.

[4] M. Sharma, D. Chadha, and V. Chandra, "High-altitude platform for free-space optical communication: Performance evaluation and reliability analysis," *J. Opt. Commun. Netw.,* vol. 8, no. 8, pp. 600–609, 2016.

[5] Y. Zeng, R. Zhang, and T. J. Lim, "Wireless communications with unmanned aerial vehicles: Opportunities and challenges," *IEEE Commun. Mag.*, vol. 54, no. 5, pp. 36–42, May 2016.

[6] M. Alzenad, M. Z. Shakir, H. Yanikomeroglu, and M.-S. Alouini, "FSO-based vertical backhaul/fronthaul framework for 5G + wireless networks," *IEEE Commun. Mag.*, vol. 56, no. 1, pp. 218–224, Jan. 2018.

[7] M. Li, Y. Hong, C. Zeng, Y. Song, and X. Zhang, "Investigation on the UAV-to-satellite optical communication systems," *IEEE J. Sel. Areas Commun.*, vol. 36, no. 9, pp. 2128–2138, Sep. 2018.

[8] V. V. Mai and H. Kim, "Beam size optimization and adaptation for high-altitude airborne free-space optical communication systems," *IEEE Photon. J.*, vol. 11, no. 2, pp. 1–13, Apr. 2019.

[9] H. Safi, A. Dargahi, J. Cheng, and M. Safari, "Analytical channel model and link design optimization for ground-to-HAP free-space optical communications," *IEEE/OSA J. Lightw. Technol.*, vol. 38, no. 18, pp. 5036–5047, Sep. 2020.

[10] W. Guo, Y. Zhan, T. A. Tsiftsis, and L. Yang, "Performance and channel modeling optimization for hovering UAV-assisted FSO links," *IEEE/OSA J. Lightw. Technol.*, vol. 40, no. 15, pp. 4999–5012, Aug. 2022.

[11] G. K. Kurt et al., "A vision and framework for the high altitude platform station (HAPS) networks of the future," *IEEE Commun. Surveys Tuts.*, vol. 23, no. 2, pp. 729–779, Apr.–Jun. 2021.

[12] Y. Ata and M.-S. Alouini, "HAPS based FSO links performance analysis and improvement with adaptive optics correction," 2022. [Online]. Available: https://www.techrxiv.org/articles/preprint/HAPS_based_FSO_Links_Performance_Analysis_and_Improvement_with_Adaptive_Optics_Correction/20324421/1

[13] R. Swaminathan, S. Sharma, N. Vishwakarma, and A. Madhukumar, "HAPS-based relaying for integrated space-air-ground networks with hybrid FSO/RF communication: A performance analysis," *IEEE Trans. Aerosp. Electron. Syst.*, vol. 57, no. 3, pp. 1581–1599, Jun. 2021.

[14] R. Samy, H.-C. Yang, T. Rakia, and M.-S. Alouini, "Performance analysis of hybrid SAG-FSO/RF satellite communication system," 2022. [Online]. Available: https://www.techrxiv.org/articles/preprint/Performance_Analysis_of_Hybrid_SAG-FSO_RF_Satellite_Communication_System/19623849

[15] R. Barrios and F. Dios, "Exponentiated weibull distribution family under aperture averaging for Gaussian beam waves," *Opt. Exp.*, vol. 20, no. 12, pp. 13055–13064, 2012.

[16] F. S. Vetelino, C. Young, and L. Andrews, "Fade statistics and aperture averaging for Gaussian beam waves in moderate-to-strong turbulence," *Appl. Opt.*, vol. 46, no. 18, pp. 3780–3789, 2007.

[17] N. Perlot and D. Fritzsche, "Aperture averaging: Theory and measurements," *Free-Space Laser Commun. Technol. XVI*, vol. 5338, pp. 233–242, 2004.

[18] L. C. Andrews and R. L. Phillips, "*Laser Beam Propagation through Random Media*," 2nd ed., Bellingham, Washington USA: SPIE Press, 2005.

[19] M. C. Al Naboulsi, H. Sizun, and F. de Fornel, "Fog attenuation prediction for optical and infrared waves," *Opt. Eng.*, vol. 43, no. 2, pp. 319–329, 2004.

[20] A. Viswanath, V. K. Jain, and S. Kar, "Analysis of earth-to-satellite free-space optical link performance in the presence of turbulence, beam-wander induced pointing error, and weather conditions for different intensity modulation schemes," *IET Commun.*, vol. 9, no. 18, pp. 2253–2258, 2015.

[21] M. S. Awan, E. L. Marzuki, B. Hillbrand, F. Nadeem, and M. S. Khan, "Cloud attenuations for free-space optical links," in *Proc. IEEE Int. Workshop Satell. Space Commun.*, 2009, pp. 274–278.

[22] E. Erdogan, I. Altunbas, G. K. Kurt, and H. Yanikomeroglu, "Cooperation in Space: HAPS-aided optical inter-satellite connectivity with opportunistic scheduling," *IEEE Commun. Lett.*, vol. 26, no. 4, pp. 882–886, Apr. 2022.

[23] M. V. Jamali et al., "Statistical studies of fading in underwater wireless optical channels in the presence of air bubble, temperature, and salinity random variations," *IEEE Trans. Commun.*, vol. 66, no. 10, pp. 4706–4723, Oct. 2018.

[24] W. Gappmair, S. Hranilovic, and E. Leitgeb, "OOK performance for terrestrial FSO links in turbulent atmosphere with pointing errors modeled by hoyt distributions," *IEEE Commun. Lett.*, vol. 15, no. 8, pp. 875–877, Aug. 2011.

[25] V. Adamchik and O. Marichev, "The algorithm for calculating integrals of hypergeometric type functions and its realization in REDUCE system," in *Proc. Int. Symp. Symbolic Algebr. Computation*, 1990, pp. 212–224.

[26] I. S. Gradshteyn and I. M. Ryzhik, *Table of Integrals, Series, and Products*. San Diego, CA, USA: Academic press, 2014.

[27] W. Inc., "The wolfram functions site," Accessed: Jun. 13, 2022. [Online]. Available: https://functions.wolfram.com

[28] W. Inc., "Wolfram alpha," Accessed: Jun. 13, 2022. [Online]. Available: https://www.wolframalpha.com